

CMB Probes for Cosmology and Particle Physics

Martin BUCHER

Laboratoire APC (Astroparticles & Cosmologie)

Université Paris 7 (Denis-Diderot)/CNRS

Paris, France

and

University of KwaZulu-Natal

Durban, South Africa

22 May 2019

Russian National Research Nuclear University MEPhI

Moscow, Russian Federation

Invited Lecture 12 for “Introduction to Cosmoparticle Physics” Course

Basic reference :



Cornell University
Library

[arXiv.org](#) > [astro-ph](#) > [arXiv:1501.04288](#)

Astrophysics > **Cosmology and Nongalactic Astrophysics**

Physics of the cosmic microwave background anisotropy

[Martin Bucher](#) (Laboratoire APC, Université Paris 7/CNRS, Paris, France and School of Mathematics, Statistics and Computer Science, University of KwaZulu-Natal, Durban, South Africa)

(Submitted on 18 Jan 2015)

Observations of the cosmic microwave background (CMB), especially of its frequency spectrum and its anisotropies, both in temperature and in polarization, have played a key role in the development of modern cosmology and our understanding of the very early universe. We review the underlying physics of the CMB and how the primordial temperature and polarization anisotropies were imprinted. Possibilities for distinguishing competing cosmological models are emphasized. The current status of CMB experiments and experimental techniques with an emphasis toward future observations, particularly in polarization, is reviewed. The physics of foreground emissions, especially of polarized dust, is discussed in detail, since this area is likely to become crucial for measurements of the B modes of the CMB polarization at ever greater sensitivity.

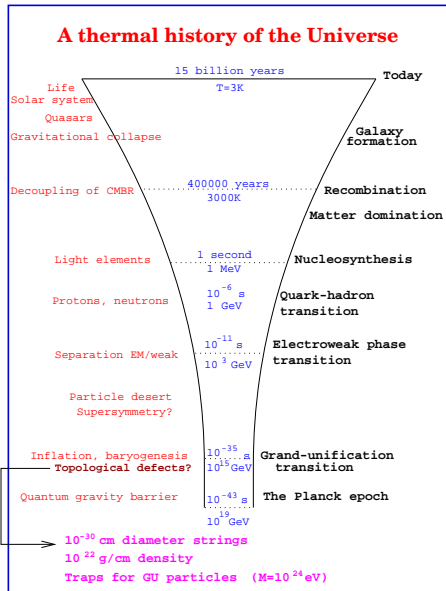
Comments: 105 pages, 26 figures

Subjects: **Cosmology and Nongalactic Astrophysics (astro-ph.CO)**

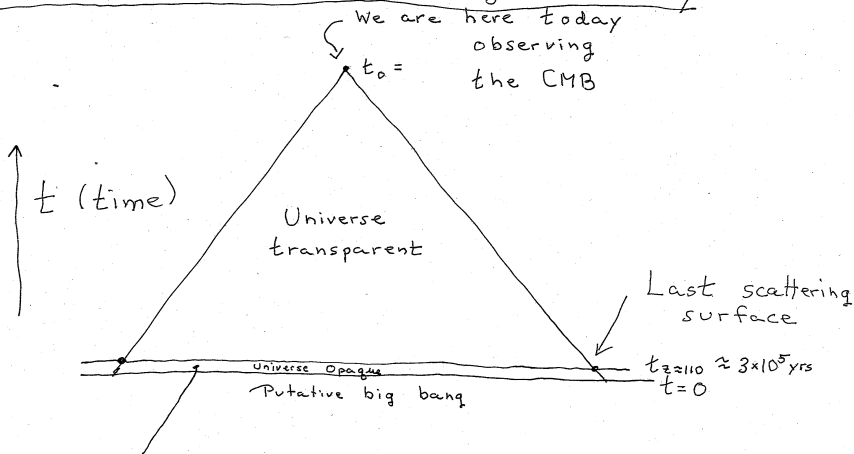
DOI: [10.1142/S0218271815300049](#)

Cite as: [arXiv:1501.04288](#) [[astro-ph.CO](#)]
(or [arXiv:1501.04288v1](#) [[astro-ph.CO](#)] for this version)

Thermal history of the Universe



CMB - What are we looking at today?



$x_e \approx 1$ Photons diffuse (random walk)

x (space)

$$ds^2 = -dt^2 + a^2(t) [dx^2 + dy^2 + dz^2]$$

$a(t) \equiv$ scale factor

Scale factors

$a(t) \sim t^{1/2}$ radiation-dominated universe (R.D.)

$a(t) \sim t^{2/3}$ matter-dominated universe (M.D.)

$a(t) \sim e^{Ht}$ vacuum-energy (cosmological constant)
dominated universe (V.D.)
[aka 'de Sitter space']

$$a(\eta) \sim \eta$$

$$a(\eta) \sim \eta^2$$

$$a(\eta) \sim \frac{1}{\eta}$$

$$\eta = \int \frac{dt}{a(t)}$$

$$ds^2 = a^2(\eta) [-d\eta^2 + d\underline{x}^2]$$
$$= -dt^2 + a^2(t) d\underline{x}^2$$

$t \equiv$ proper (clock) time

$\eta \equiv$ conformal time

Here $-\infty < \eta < 0.$

Saha equilibrium (approximate description)

$$\frac{x_e^2}{(1 - x_e)} = \frac{n_Q}{n_B} \exp \left[-\frac{E_I}{k_B T} \right]$$

where $E_I = 13.4$ eV and

$$n_Q = \left(\frac{2\pi m_e k_B T}{h^2} \right)^{3/2}.$$

We may rewrite

$$\begin{aligned} \frac{n_Q}{n} &= \frac{O(1)}{n_B} \left(\frac{m_e c^2}{k_B T} \right)^{3/2} \left(\frac{k_B T}{\hbar c} \right)^3 \\ &= O(1) \left(\frac{m_e c^2}{k_B T} \right)^{3/2} \left(\frac{n_\gamma}{n_B} \right). \end{aligned}$$

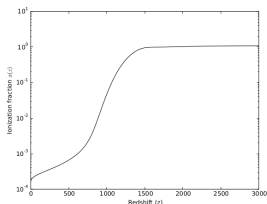


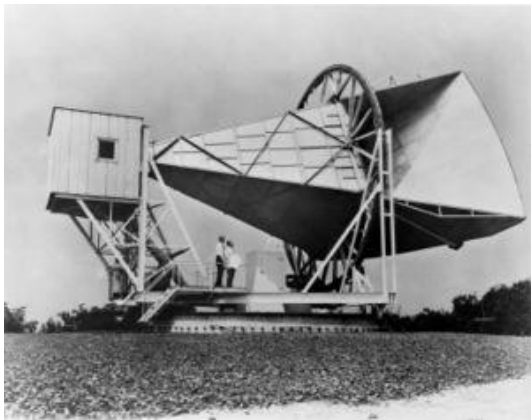
Figure 11: **Ionization fraction as function of redshift with effect of late-time ionizing radiation ignored.** Calculated using the code *Cosmo Rec* by Jens Chluba (for details see Ref. [\[213\]](#)).

Summary so far

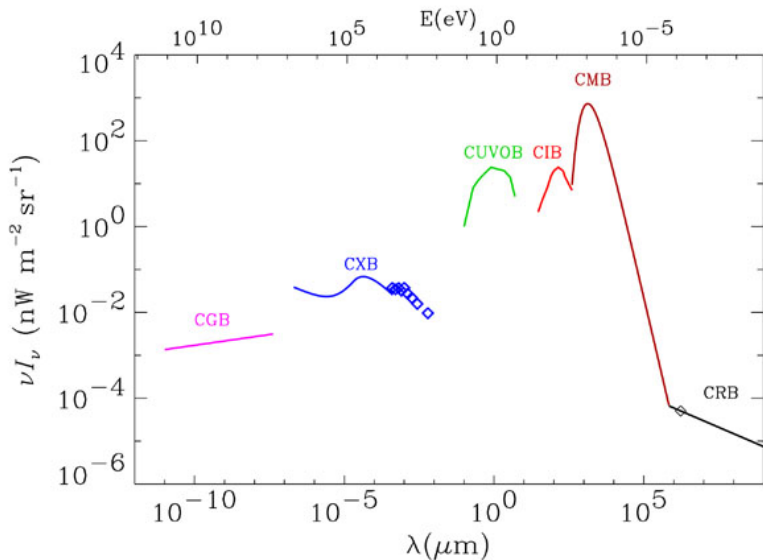
- ▶ The microwave background that we see today is a nearly perfect blackbody having a nearly isotropic temperature of 2.725 K.
- ▶ Over the almost all of the 13.82×10^9 years of cosmic history—that is, over 99.997% of this history, $\approx 94\%$ of the microwave photons propagated to us without ever being rescattered.
- ▶ Only during approximately the first 380,000 years since the putative Big Bang was scattering appreciable, before the universe cooled down, allowing the primordial plasma to transform into neutral hydrogen and helium.
- ▶ The agreement of the CMB energy spectrum with a perfect blackbody provides strong confirmation of the hot big bang model.
- ▶ The temperature fluctuations (at the level of approximately 1 part in 10^5) provide a sensitive probe of the initial conditions of our universe. Roughly speaking, observing the CMB provides a snapshot of the state the universe on a sphere of radius 45 Billion light years, almost all the way back to the putative Big Bang, at an epoch when the cosmological perturbations were small and well described by linear theory. [Question : Why does this radius exceed the age of the universe?]

Discovery of the cosmic microwave background

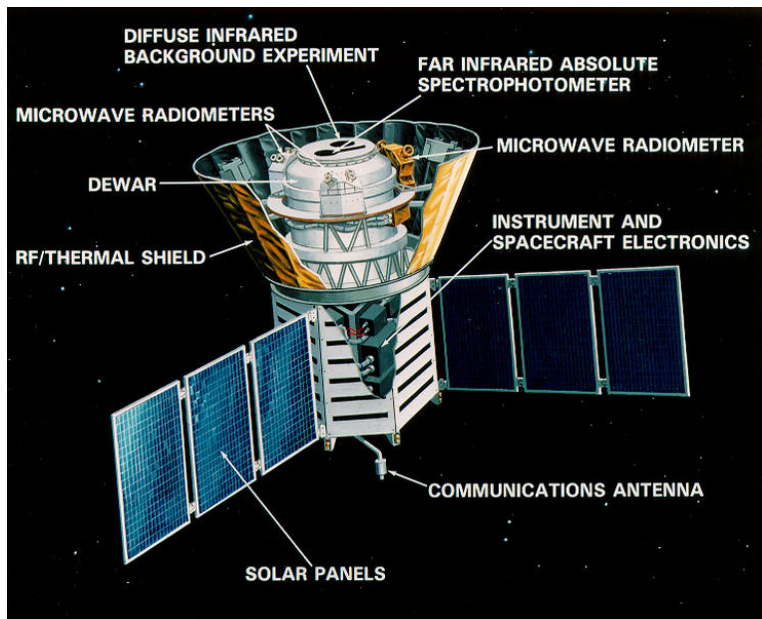
1963 Penzias and Wilson (Bell Labs) observed a background of microwaves having a thermal spectrum with $T = 2.73K$. This temperature is (almost) the same no matter what the direction in the sky.



Electromagnetic radiation energy content of Universe

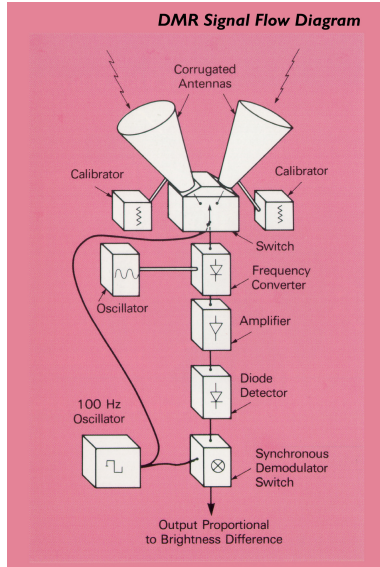


The NASA COBE Satellite

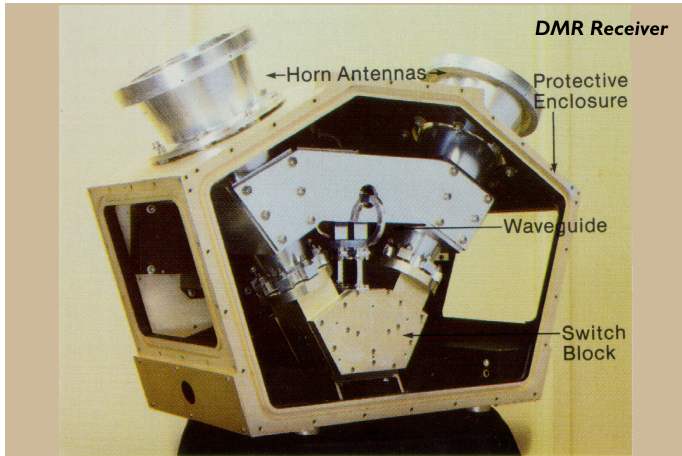


COBE DMR (Differential Microwave Radiometers)

Instrument block diagram

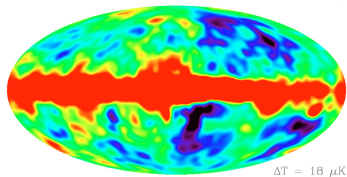
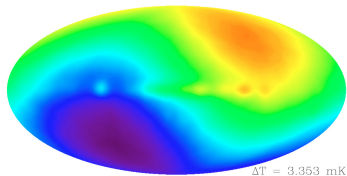


The DMR Instrument

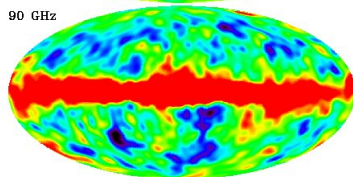
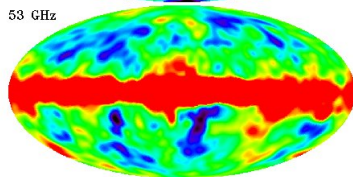
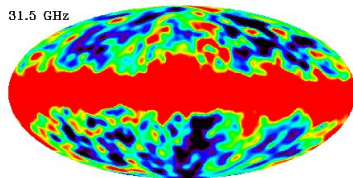


Raw COBE CMB Maps with Successive Subtractions

DMR 53 GHz Maps



COBE DMR (Differential Microwave Radiometers) Frequency Maps



-100 μK  +100 μK

How best to interpret the maps?

Two-point function of an isotropic Gaussian random process.

$$\delta T(\hat{\mathbf{n}}) = \sum_{\ell=0}^{\infty} \sum_{m=-\ell}^{+\ell} a_{\ell m} Y_{\ell m}(\hat{\mathbf{n}})$$

$$\langle a_{\ell m}^* a_{\ell' m'} \rangle = \delta_{\ell \ell'} \delta_{m m'} c_{\ell}$$

$$c_{\ell}^{(sky)} = \frac{1}{(2\ell + 1)} \sum_{m=-\ell}^{+\ell} |a_{\ell m}|^2$$

Cosmic Variance — We have only one sky to observe

$c_\ell^{(sky)}$ obeys a χ^2 distribution with $(2\ell + 1)$ degrees of freedom.

Probability of CMB temperature sky map given a theory

$$P\left(\{a_{\ell m}\} \middle| \{c_\ell^{(th)}\}\right) = \prod_{\ell=0}^{\infty} \prod_{m=-\ell}^{+\ell} \frac{1}{\sqrt{2\pi c_\ell^{(th)}}} \exp\left[-\frac{1}{2} |a_{\ell m}|^2\right]$$

Or we can express the result in terms of a log likelihood

$$\ln P\left(\{c_\ell^{(obs)}\} \middle| \{c_\ell^{(th)}\}\right) = \sum_{\ell=0}^{\infty} (2\ell + 1) \left(\frac{C_{obs}}{C_{th}} - 1 + \ln\left(\frac{C_{obs}}{C_{th}}\right) \right) + (\text{constant})$$

Error due to cosmic variance :

$$\left(\frac{\delta c_\ell}{c_\ell}\right)_{obs} = \sqrt{\frac{2}{2\ell + 1}}$$

COBE DMR angular power spectrum

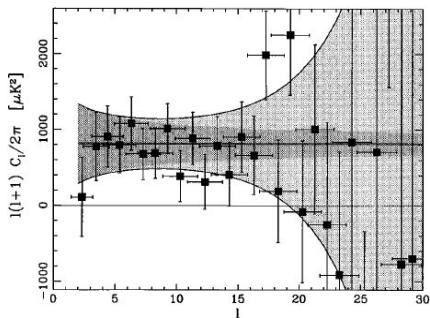
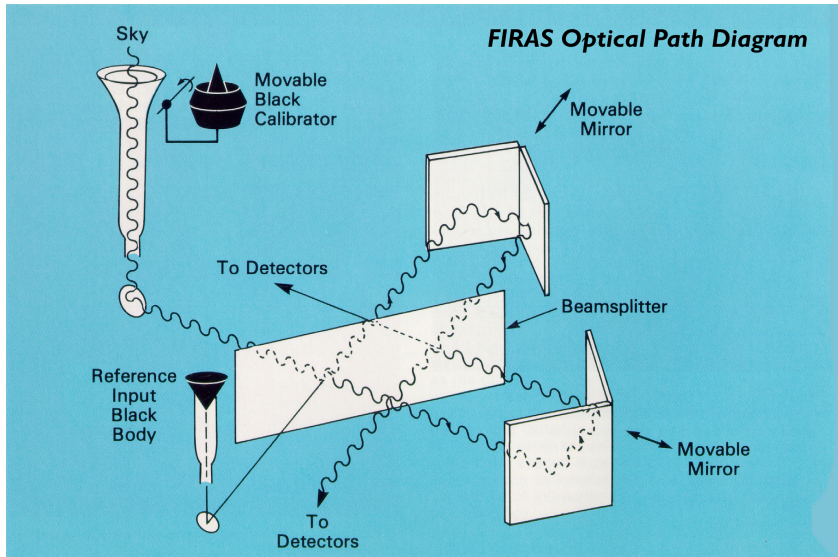


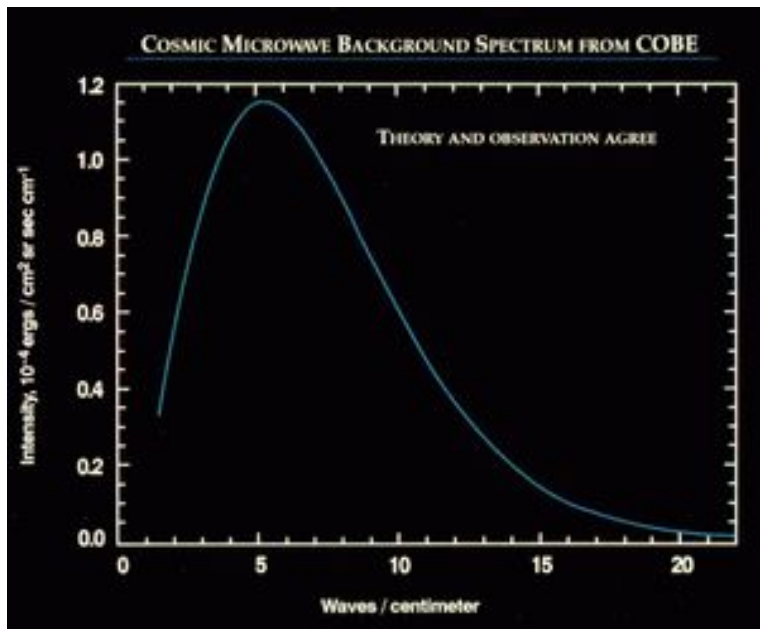
FIG. 1.—Power spectrum observed by *COBE*. The observed multipoles $D_\ell = \ell(\ell + 1)C_\ell$ are plotted with 1σ error bars. The vertical error bars include both pixel noise and cosmic variance, and the horizontal bars show the width of the window functions used. If the true power spectrum is given by $n = 1$ and $Q_{\text{rms, ps}} = 18.4 \mu K$ (heavy horizontal line), then the shaded region gives the 1σ error bars and the dark-shaded region shows the contribution from cosmic variance.

From Tegmark (1996)

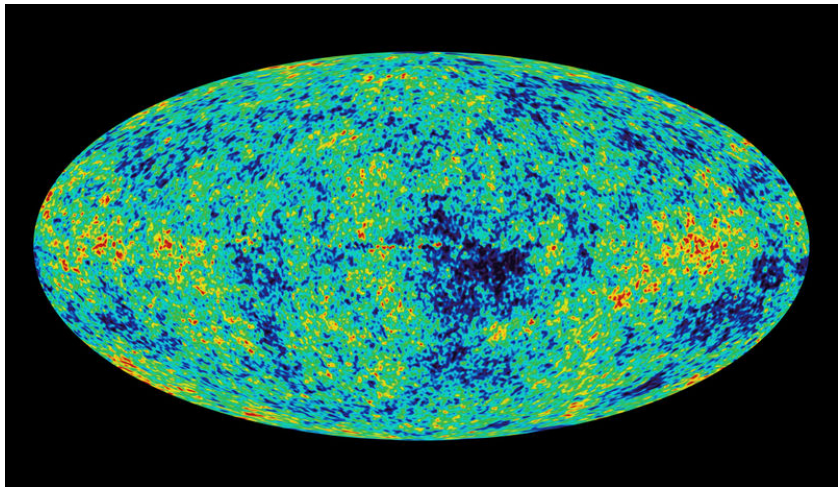
FIRAS Instrument Concept



FIRAS Determination of Frequency Spectrum



Preview of WMAP



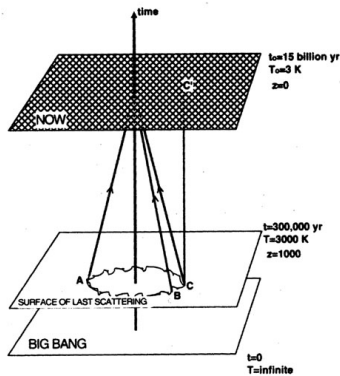
Theory – Origin of the CMB anisotropy

Sachs-Wolfe formula

$$\frac{\delta T}{T}(\hat{\mathbf{n}}) = \left[\frac{1}{4} \delta_\gamma + \mathbf{v}_\gamma \cdot \mathbf{n} + \Phi \right]_i^f + 2 \int_i^f d\eta \frac{\partial \Phi'}{\partial \eta}(\eta, \hat{\mathbf{n}}(\eta_0 - \eta))$$

$\Phi \equiv$ Newtonian gravitational potential (dimensionless)

δ_γ and \mathbf{v}_γ describe the fractional density contrast and peculiar 3-velocity of the photon component.



This treatment is somewhat naive because it assumes that the surface of last scatter is infinitely thin.

In reality the surface of last scatter has a width that smears the anisotropies on small scales.

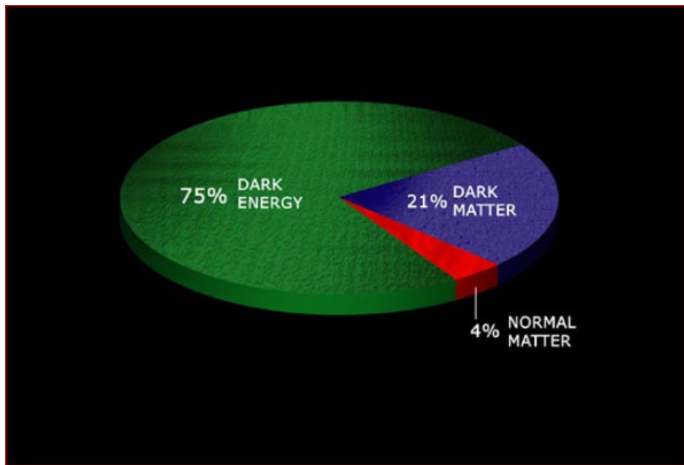
CMB Anisotropies - Toward a More Careful Treatment

A exact treatment must keep track of both photon polarizations and the entire angular distribution function, which requires in principle an infinite number of variables. Here are the photon equations :

$$\begin{aligned}\dot{\delta}_\gamma &= -\frac{4}{3}\dot{\theta}_\gamma + 4\dot{\phi}, \\ \dot{\theta}_\gamma &= k^2 \left(\frac{1}{4}\delta_\gamma - \sigma_\gamma \right) + k^2\psi + an_e\sigma_T(\theta_b - \theta_\gamma), \\ \dot{F}_{\gamma 2} &= 2\dot{\sigma}_\gamma = \frac{8}{15}\dot{\theta}_\gamma - \frac{3}{5}kF_{\gamma 3} - \frac{9}{5}an_e\sigma_T\sigma_\gamma + \frac{1}{10}an_e\sigma_T(G_{\gamma 0} + G_{\gamma 2}), \\ \dot{F}_{\gamma l} &= \frac{k}{2l+1} \left[lF_{\gamma(l-1)} - (l+1)F_{\gamma(l+1)} \right] - an_e\sigma_T F_{\gamma l}, \quad l \geq 3 \\ \dot{G}_{\gamma l} &= \frac{k}{2l+1} \left[lG_{\gamma(l-1)} - (l+1)G_{\gamma(l+1)} \right] + an_e\sigma_T \left[-G_{\gamma l} + \frac{1}{2}(F_{\gamma 2} + G_{\gamma 0} + G_{\gamma 2}) \left(\delta_{l0} + \frac{\delta_{l2}}{5} \right) \right]\end{aligned}$$

These are not very enlightening and accurate calculations are carried out using codes like CAMB (or CLASS). Nevertheless simplified treatments are essential for gaining intuition and understanding the output of numerical results.

Components of the Present Mean Energy Density of the Universe



Ingredients for Modelling the CMB Multipole Spectrum

Component contributing to the stress-energy-momentum tensor :

- ▶ Baryons (protons, nuclei, and accompanying electrons) Strong coupling to photons provide springiness. Pressure prevents gravitational clustering
- ▶ Neutrinos (collisionless, do not scatter)
- ▶ Photons. Relativistic. Initially tightly coupled to baryons, and cannot go anywhere because of Thomson scattering. After plasma disappears due to recombination to neutral atomic Hydrogen and Helium, the photons travel along geodesics.
- ▶ Dark matter (collisionless non-relativistic component, or cold dust) Can cluster before baryons because does not scatter with photons.
- ▶ Dark energy or cosmological constant

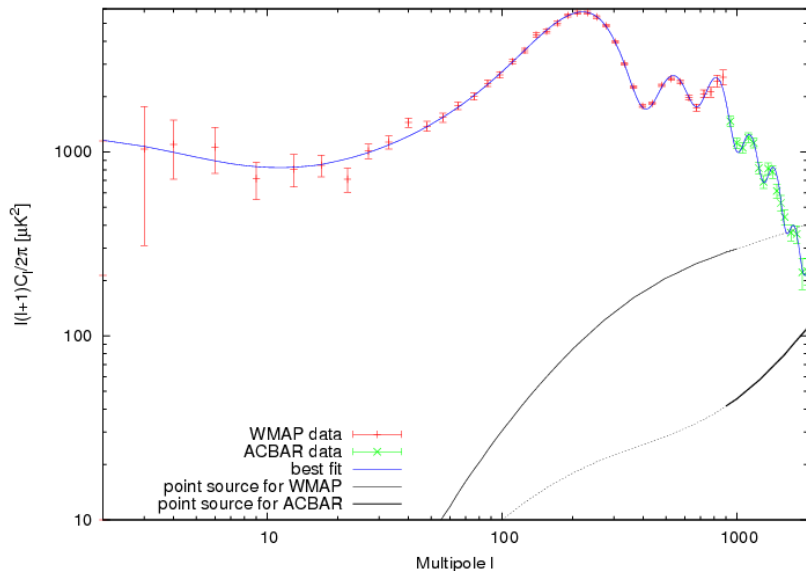
Primordial power spectrum :

$$P(k) = A_S(k/k^*)^{n_s} \text{ where } k^* \text{ is the pivot scale.}$$

Parameters :

$$H_0, \omega_b = h^2\Omega_b, \omega_{cdm} = h^2\Omega_{cdm}, \Omega_\Lambda, w \text{ (optional), } n_s, \tau_{reion}$$

Simple model fitted to WMAP and ACBAR



WMAP Cosmological Parameters

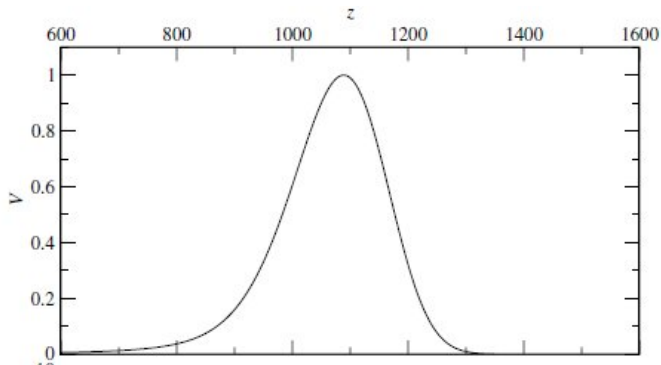
Model: Λ cdm+sz+lens

Data: wmap5

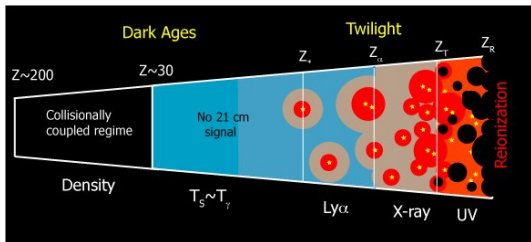
$10^2\Omega_b h^2$	2.273 ± 0.062	$1 - n_s$	$0.037^{+0.015}_{-0.014}$
$1 - n_s$	$0.0081 < 1 - n_s < 0.0647$ (95% CL)	$A_{\text{BAO}}(z = 0.35)$	0.457 ± 0.022
C_{220}	5756 ± 42	$d_A(z_{\text{eq}})$	14279^{+186}_{-189} Mpc
$d_A(z_*)$	14115^{+188}_{-191} Mpc	$\Delta_{\mathcal{R}}^2$	$(2.41 \pm 0.11) \times 10^{-9}$
h	$0.719^{+0.026}_{-0.027}$	H_0	$71.9^{+2.6}_{-2.7}$ km/s/Mpc
k_{eq}	0.00968 ± 0.00046	ℓ_{eq}	136.6 ± 4.8
ℓ_*	$302.08^{+0.83}_{-0.84}$	n_s	$0.963^{+0.014}_{-0.015}$
Ω_b	0.0441 ± 0.0030	$\Omega_b h^2$	0.02273 ± 0.00062
Ω_c	0.214 ± 0.027	$\Omega_c h^2$	0.1099 ± 0.0062
Ω_Λ	0.742 ± 0.030	Ω_m	0.258 ± 0.030
$\Omega_m h^2$	0.1326 ± 0.0063	$r_{\text{hor}}(z_{\text{dec}})$	286.0 ± 3.4 Mpc
$r_s(z_d)$	153.3 ± 2.0 Mpc	$r_s(z_d)/D_v(z = 0.2)$	0.1946 ± 0.0079
$r_s(z_d)/D_v(z = 0.35)$	0.1165 ± 0.0042	$r_s(z_*)$	146.8 ± 1.8 Mpc
R	1.713 ± 0.020	σ_8	0.796 ± 0.036
A_{SZ}	$1.04^{+0.96}_{-0.69}$	t_0	13.69 ± 0.13 Gyr
τ	0.087 ± 0.017	θ_*	0.010400 ± 0.000029
θ_*	0.5959 ± 0.0017 °	t_*	380081^{+5843}_{-5841} yr
z_{dec}	1087.9 ± 1.2	z_d	1020.5 ± 1.6
z_{eq}	3176^{+151}_{-150}	z_{reion}	11.0 ± 1.4
z_*	1090.51 ± 0.95		

Visibility function

From what redshift are the CMB photons coming (i.e., redshift of last scatter) ?

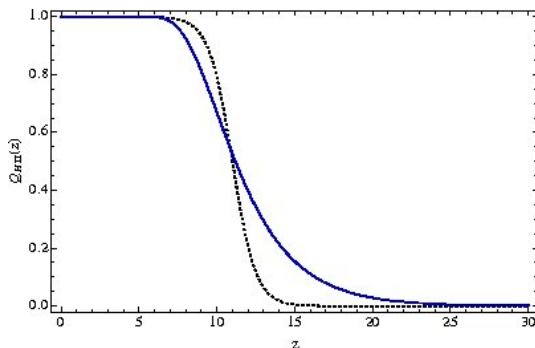


Reionization of the neutral hydrogen at intermediate redshift



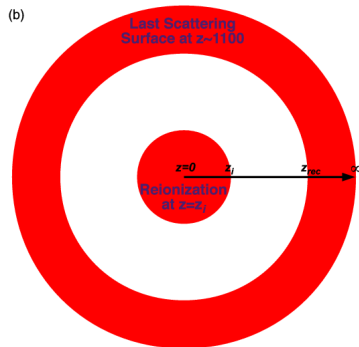
The first stars and quasars generate ionizing UV photons transforming the neutral hydrogen into free protons, ^4He nuclei, and electrons.

Possible reionization histories



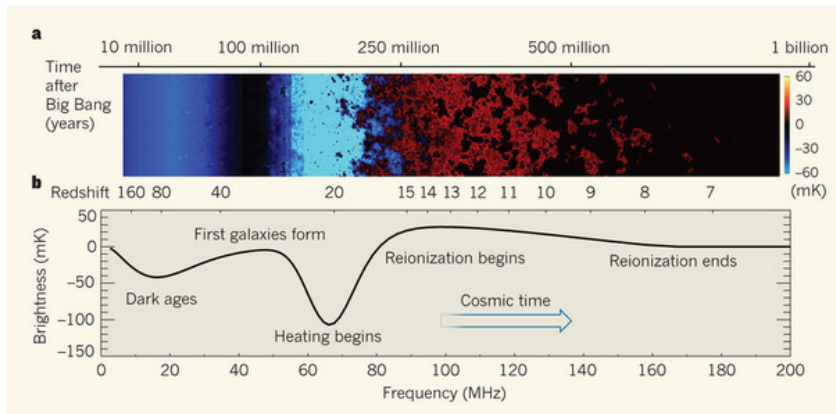
We do not know what the precise average reionization history is. It is described by a function $\tau(z)$. But the CMB has little sensitivity to the precise shape of this function, and often τ is modelled under the approximation of instantaneous reionization.

Effect of Reionization on the CMB Anisotropies

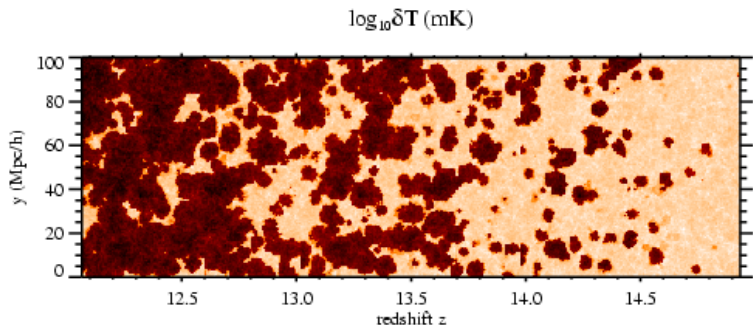


A CMB photon has a chance $\exp(-\tau)$ of remaining unscattered. This component maintains its original anisotropies from the surface of last scatter. For fraction $(1 - \exp(-\tau))$ of the photons that are recently rescattered (i.e., after 'last scattering'), all the CMB anisotropy is erased except for the anisotropy on the very largest scales

Inhomogeneous Reionization



Reionization Simulations (for Future 21cm Observations)



The following animations of the shape of the CMB spectrum as a function of the various cosmological parameters are courtesy of Wayne Hu, University of Chicago

background.uchicago.edu/~whu/

Dependence of C_{TT} on Ω_b animation

Dependence of C_{TT} on Ω_k animation

Dependence of C_{TT} on $\omega_b = h^2 \Omega_b$ animation

Dependence of C_{TT} on $\omega_{cdm} = h^2 \Omega_{cdm}$ Animation

Dependence of C_{TT} on Ω_{cdm} animation

Dependence of C_{TT} on τ animation

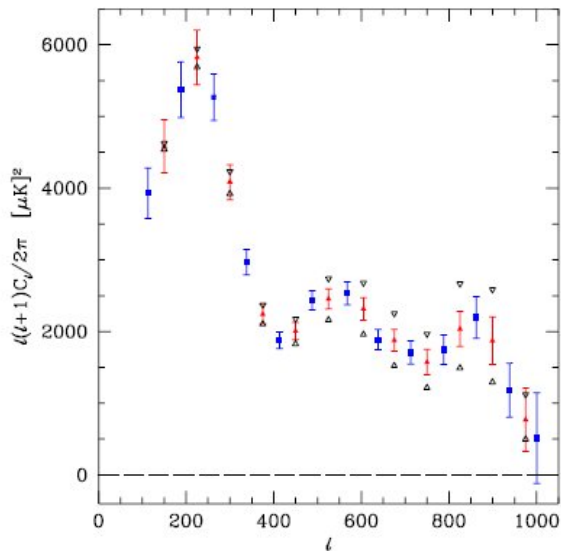
Boomerang Instrument



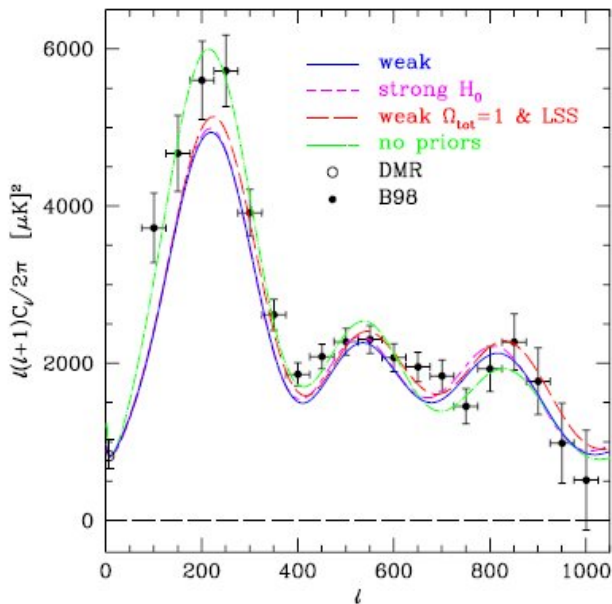
Boomerang Balloon



Boomerang Multipole Spectrum (no theory)



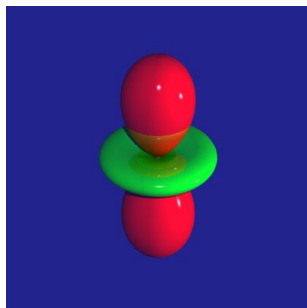
Boomerang Multipole Spectrum (with theory)



CMB Polarization

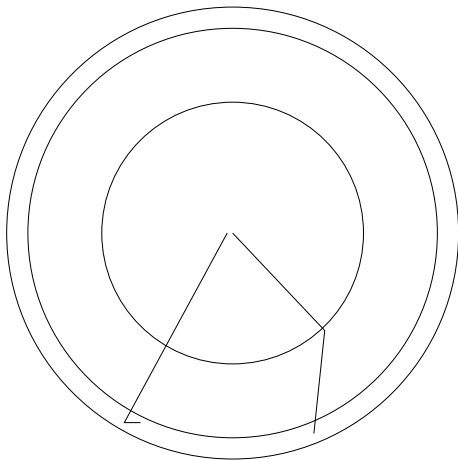
Polarized Thomson scattering ($\gamma + e^- \rightarrow \gamma + e^-$) is anisotropic.

$$\sigma_{Thomson} \propto (\epsilon_{in} \cdot \epsilon_{out})^2$$

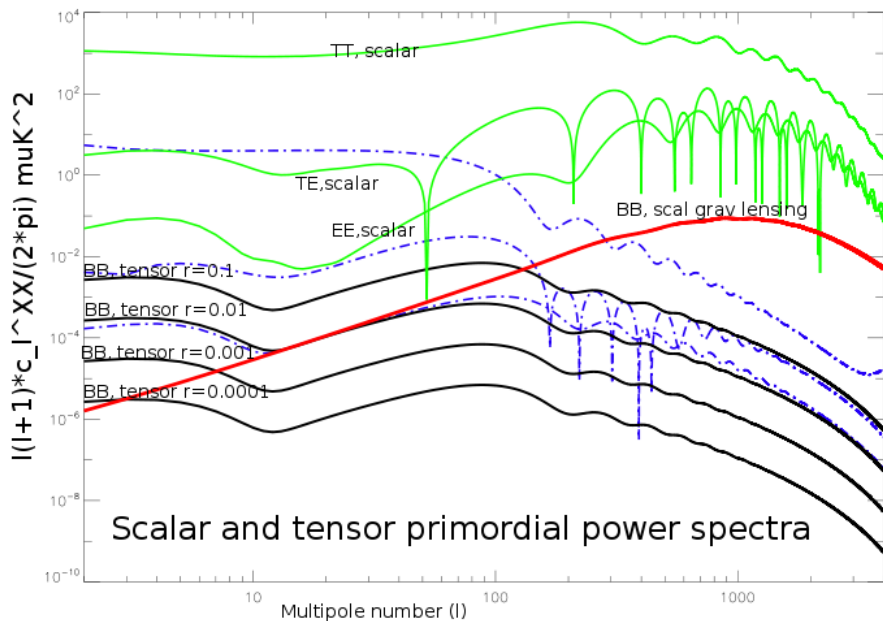


When we look at the polarization of the CMB today, we measure (roughly speaking) the CMB quadrupole seen by the electron at last scattering, which may be due to (1) intrinsic temperature fluctuations, (2) gravitational redshift, or (3) Doppler shift from shear of the velocity field.

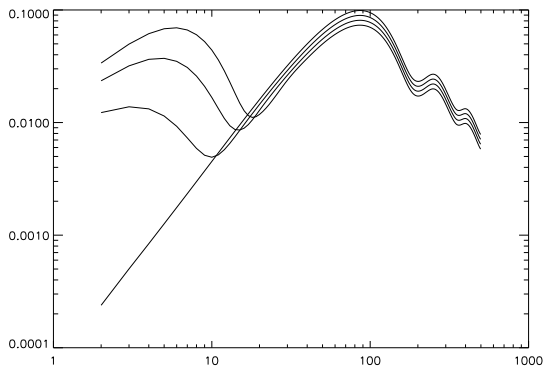
Finite width of surface of last scatter gives rise to polarization of the CMB



Roughly speaking the polarization is a measure of the quadrupole as seen by the electron of last scatter.

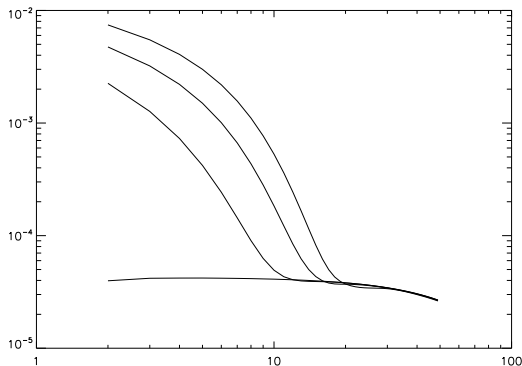


The Reionization Bump (I)



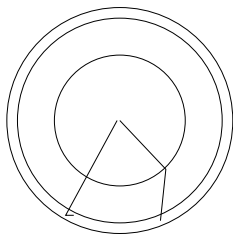
$\tau = 0.0, 0.05, 0.10, 0.15$ (bottom \rightarrow top)

The Reionization Bump (II)



Amplification of the B mode signal relative to the non reionized case by a factor of about 50, 100, and 150 at $\tau = 0.05$, $\tau = 0.10$, and $\tau = 0.15$, respectively.

The Reionization Bump (III)



It turns out that

$$P \propto (1 - \tau) d_{\text{lastscatter}}^2 \frac{\partial^2 T}{\partial x^2}$$

is small compared to

$$P \propto \tau d_{\text{reion}}^2 \frac{\partial^2 T}{\partial x^2}$$

even when τ is small.

Sources of the CMB polarization (known and possible)

- ▶ E-mode polarization
 - ▶ Scalar modes (presumably from inflation) (already seen)
 - ▶ Tensor modes (presumably from inflation) (not yet seen)
 - ▶ Cosmic strings, more generally any non-linear late time source (speculative)
 - ▶ Polarized foreground emission (galactic dust, synchrotron, IR galaxies, spinning dust,.....) (seen but not well characterized)
- ▶ B mode polarization
 - ▶ Tensor modes (presumably from inflation) (not yet seen)
 - ▶ Gravitational lensing ($E + \Phi \rightarrow B$) (not yet seen, but certainly there and well understood and calculable)
 - ▶ Polarized foreground emission (galactic dust, synchrotron, IR galaxies, spinning dust,.....) (seen but not well characterized)
 - ▶ Cosmic strings, more generally any non-linear late time source (speculative)
 - ▶ Magnetic fields at recombination ($E \rightarrow B$ Faraday rotation) (speculative)
 - ▶ Something else (?)

E and B Mode Polarization



E mode

B mode

$$\mathbf{Y}_{\ell m, ab}^{(E)} = \sqrt{\frac{2}{(\ell-1)\ell(\ell+1)(\ell+2)}} \left[\nabla_a \nabla_b - \frac{1}{2} \delta_{ab} \nabla^2 \right] Y_{\ell m}(\hat{\Omega})$$

$$\mathbf{Y}_{\ell m, ab}^{(B)} = \sqrt{\frac{2}{(\ell-1)\ell(\ell+1)(\ell+2)}} \frac{1}{2} \left[\epsilon_{ac} \nabla_c \nabla_b + \nabla_a \epsilon_{bc} \nabla_c \right] Y_{\ell m}(\hat{\Omega})$$

Projection of 'scalars,' 'vectors' and 'tensors' onto the celestial sphere

Under projection onto the celestial sphere :

$$(scalar)_3 \rightarrow (scalar)_2,$$

$$(vector)_3 \rightarrow (scalar)_2 + (vector)_2,$$

$$(tensor)_3 \rightarrow (scalar)_2 + (vector)_2.$$

There is no $(tensor)_2$ component. The E mode polarization is scalar; the B mode is vector.

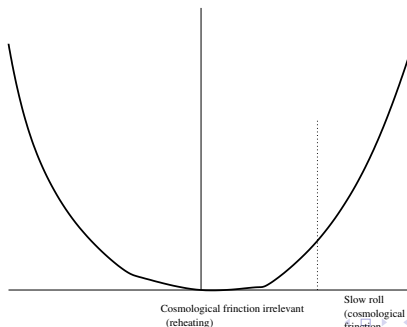
It follows that at linear order the scalar modes cannot generate any B mode polarization.

Note crucial role of linearity assumption.

Single-Field Inflation

In the beginning there was a scalar field that dominated the universe. Everything came from this scalar field and there was nothing without the scalar field. The quantum fluctuations of this field (that is, those of the vacuum) generated small fluctuations that advanced or retarded the instant of re-heating. These were the seeds of the large-scale structure.

$$\ddot{\phi} + 3H\dot{\phi} = -V_{,\phi}$$



Perturbations generated during inflation

$$\boxed{\hbar = c = 1, M_{pl}^{-2}} \quad \delta\phi \approx H \quad \frac{\delta\rho}{\bar{\rho}} \approx H \cdot \delta t, \quad \delta t \approx \frac{\delta\phi}{\dot{\phi}}$$

$$H\dot{\phi} \approx V_{,\phi}, \quad \dot{\phi} \approx V_{,\phi}/H, \quad H^2 \approx \frac{1}{M_{pl}^2} V, \quad \frac{\delta\rho}{\bar{\rho}} \approx \frac{V^{3/2}[\phi(k)]}{M_{pl}^3 V_{,\phi}}$$

Scalar perturbations :

$$\mathcal{P}_S^{1/2}(k) \approx O(1) \cdot \frac{V^{3/2}[\phi(k)]}{M_{pl}^3 V_{,\phi}[\phi(k)]}.$$

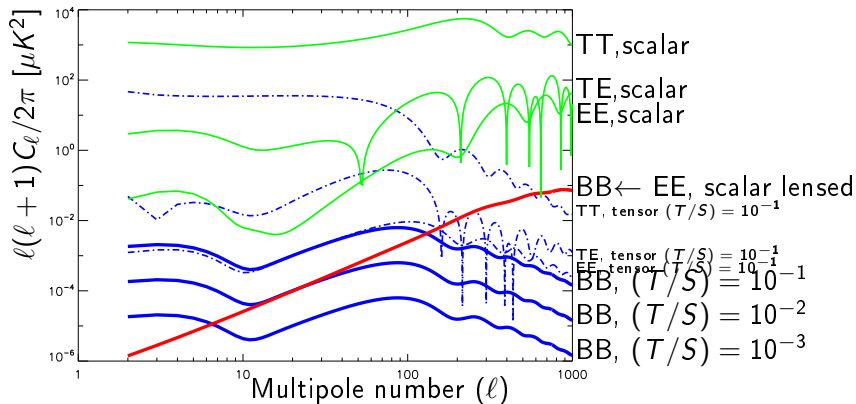
Tensor perturbations :

$$\mathcal{P}_T^{1/2}(k) \approx O(1) \cdot \frac{H}{M_{pl}} \approx O(1) \cdot \frac{V^{1/2}}{M_{pl}^2}$$

$\phi(k) \equiv$ value of ϕ at horizon crossing of the mode k

Reconstruction of the inflationary potential : the tensors measure the height of the potential, the scalars the slope.

Inflationary Prediction for Scalar & Tensor Anisotropies



Lensing of the E mode into the B mode — ($E^{scalar} + \Phi \rightarrow B^{scalar}$)

(Flat sky approximation : $(\ell m) \rightarrow \ell$, $\theta, \ell \in \mathcal{R}^2$.)

$$\delta\theta = (\nabla\Phi), \quad \delta T(\theta) = (\nabla\Phi) \cdot (\nabla T).$$

$$\delta T(\ell_F) = \int \frac{d^2\ell_L}{(2\pi)^2} (-\ell_L) \cdot (\ell_F - \ell_L) \Phi(\ell_L) T(\ell_F - \ell_L).$$

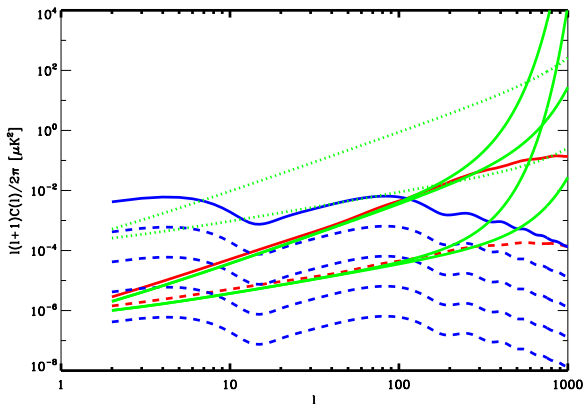
$$\langle T(\ell) T(\ell') \rangle = (2\pi)^2 \delta^2(\ell + \ell') C^{TT}(\ell)$$

$$C^{TT}(\ell_F) = \int \frac{d^2\ell_L}{(2\pi)^2} [\ell_L \cdot (\ell_F - \ell_L)]^2 C^{\Phi\Phi}(\ell_L) C^{TT}(\ell_I = |\ell_F - \ell_L|)$$

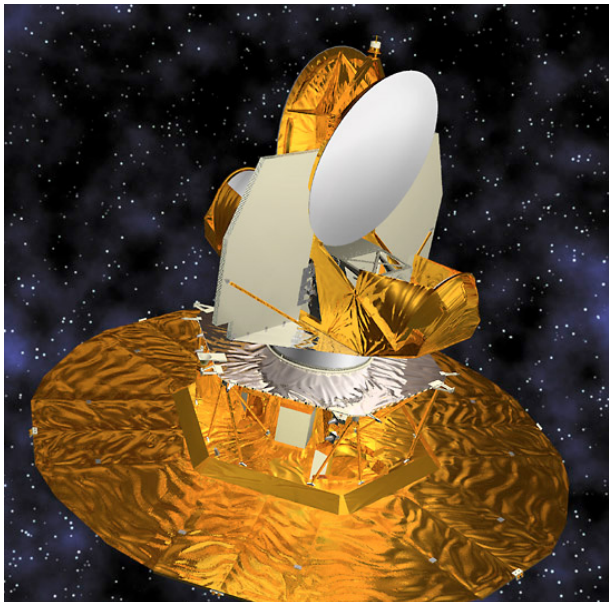
$$C^{BB}(\ell_B) = \int \frac{d^2\ell_L}{(2\pi)^2} [\ell_L \cdot (\ell_F - \ell_L)]^2 \sin^2[2\Theta(\ell_B, \ell_E)] C^{\Phi\Phi}(\ell_L) C^{EE}(\ell_E = |\ell_B - \ell_L|)$$

The detection of B modes

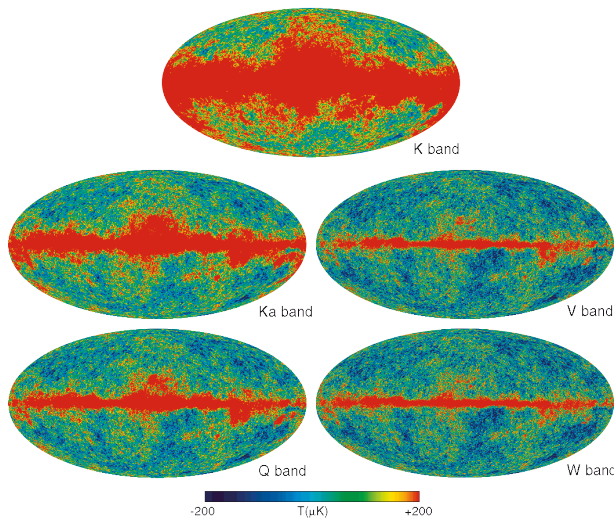
The B mode is that component that cannot be represented as a double gradient on the celestial sphere. In the linear approximation there is no B mode component arising from scalar degrees of freedom. The presence of the B mode would unambiguously signal the presence of primordial gravitational waves.



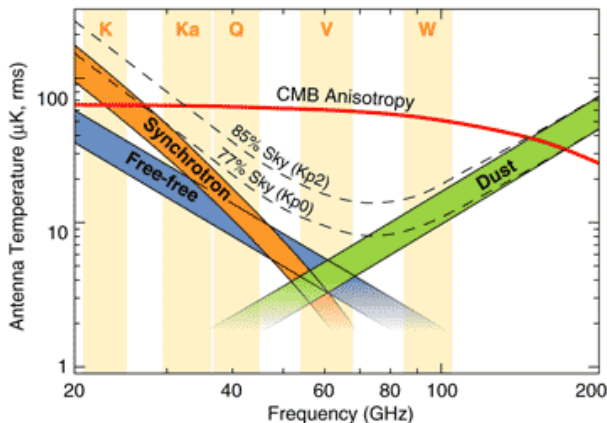
NASA WMAP Space Mission (launched 30 June 2001,
mission length almost 11 yrs.)



WMAP Temperature Anisotropy Maps

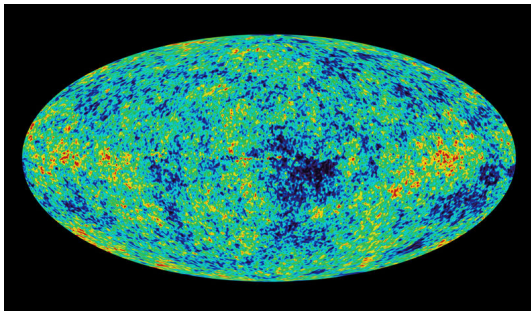


Microwave Foreground Frequency Spectra

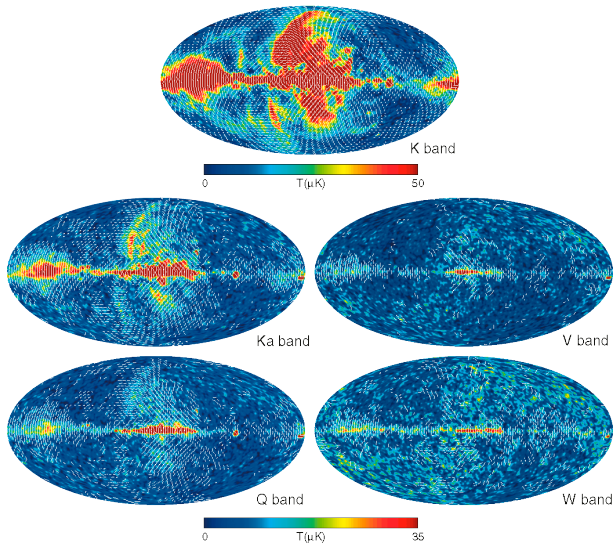


There is a narrow window in frequency ranging from around 40 GHz to 150 GHz within which the CMB anisotropies dominate over other astrophysical foreground components.

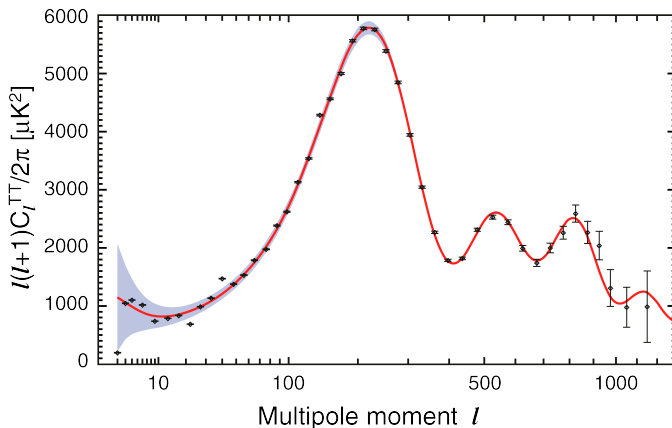
WMAP Temperature Anisotropy Maps



WMAP Polarization Anisotropy Maps

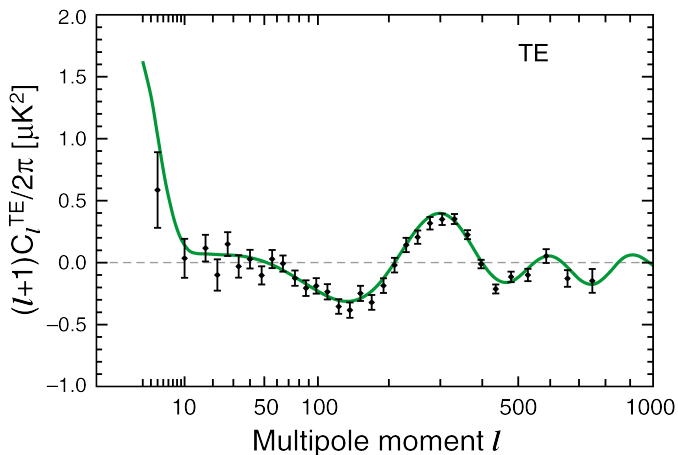


WMAP Temperature Power Spectrum

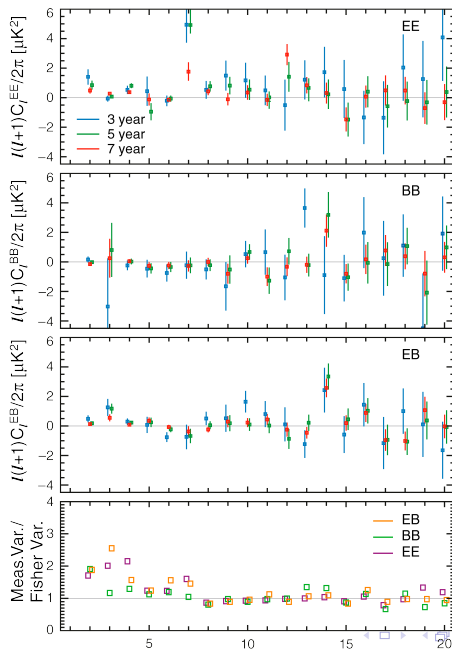


$$T(\hat{\Omega}) = \sum_{\ell=0}^{\infty} \sum_{m=-\ell}^{+\ell} a_{\ell m} Y_{\ell m}(\theta, \phi), \quad c_{\ell} = \langle |a_{\ell m}|^2 \rangle$$

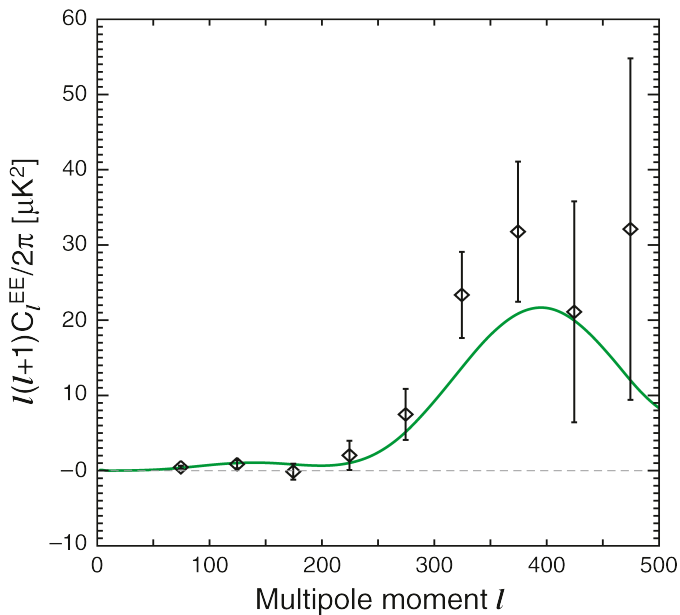
WMAP Temperature-E mode polarization cross power spectrum



WMAP polarization power spectrum (low- ℓ)



WMAP E-mode polarization power spectrum (high- ℓ)

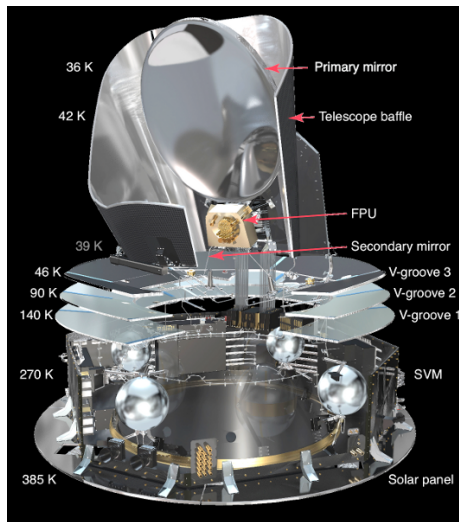


WMAP 7-year best-fit cosmological parameters

WMAP Cosmological Parameters				
Model: Λ cdm+sz+lens				
Data: wmap7+bao+h0				
$10^2\Omega_b h^2$	2.260 ± 0.053	$1 - n_s$	0.037 ± 0.012	
$1 - n_s$	$0.013 < 1 - n_s < 0.061$ (95% CL)	$A_{\text{BAO}}(z = 0.35)$	0.468 ± 0.011	
C_{220}	5762^{+38}_{-37}	$d_A(z_{\text{eq}})$	14238^{+128}_{-129} Mpc	
$d_A(z_*)$	14073^{+129}_{-130} Mpc	$\Delta^2_{\mathcal{R}}$	$(2.441^{+0.088}_{-0.092}) \times 10^{-9}$	
h	$0.704^{+0.013}_{-0.014}$	H_0	$70.4^{+1.3}_{-1.4}$ km/s/Mpc	
k_{eq}	0.00985 ± 0.00026	ℓ_{eq}	$138.6^{+2.6}_{-2.5}$	
ℓ_*	302.40 ± 0.73	n_s	0.963 ± 0.012	
Ω_b	0.0456 ± 0.0016	$\Omega_b h^2$	0.02260 ± 0.00053	
Ω_c	0.227 ± 0.014	$\Omega_c h^2$	0.1123 ± 0.0035	
Ω_Λ	$0.728^{+0.015}_{-0.016}$	Ω_m	$0.272^{+0.016}_{-0.015}$	
$\Omega_m h^2$	0.1349 ± 0.0036	$r_{\text{hor}}(z_{\text{dec}})$	284.6 ± 1.9 Mpc	
$r_s(z_d)$	152.7 ± 1.3 Mpc	$r_s(z_d)/D_v(z = 0.2)$	$0.1904^{+0.0037}_{-0.0038}$	
$r_s(z_d)/D_v(z = 0.35)$	0.1143 ± 0.0020	$r_s(z_*)$	146.2 ± 1.1 Mpc	
R	$1.7239^{+0.0100}_{-0.0099}$	σ_8	0.809 ± 0.024	
A_{SZ}	$0.96^{+0.69}_{-0.96}$	t_0	13.75 ± 0.11 Gyr	
τ	0.087 ± 0.014	θ_*	0.010389 ± 0.000025	
θ_*	0.5953 ± 0.0014 °	t_*	377730^{+3205}_{-3200} yr	
z_{dec}	1088.2 ± 1.1	z_d	1020.5 ± 1.3	
z_{eq}	3232 ± 87	z_{reion}	10.4 ± 1.2	
z_*	$1090.89^{+0.68}_{-0.69}$			

The Planck satellite

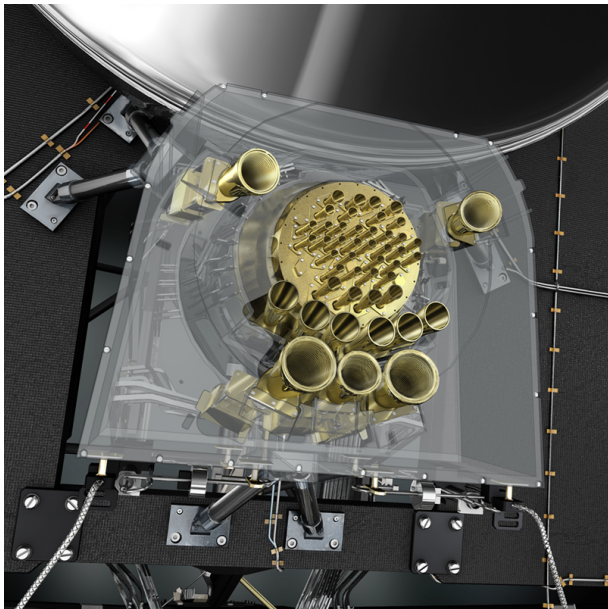
(launched 13 May 2009, 30 months of data taken)



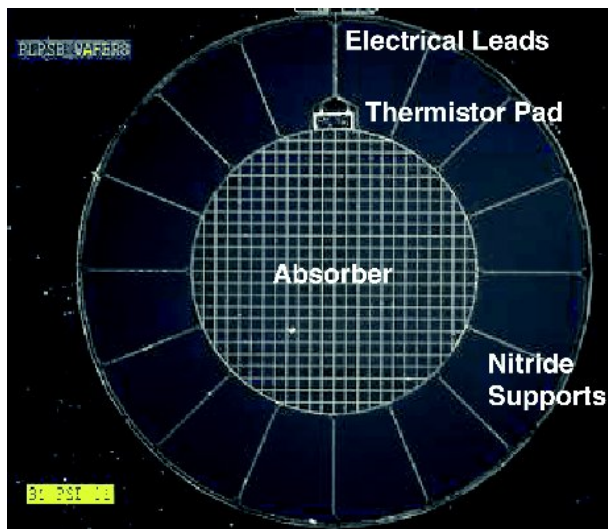
Planck collaboration



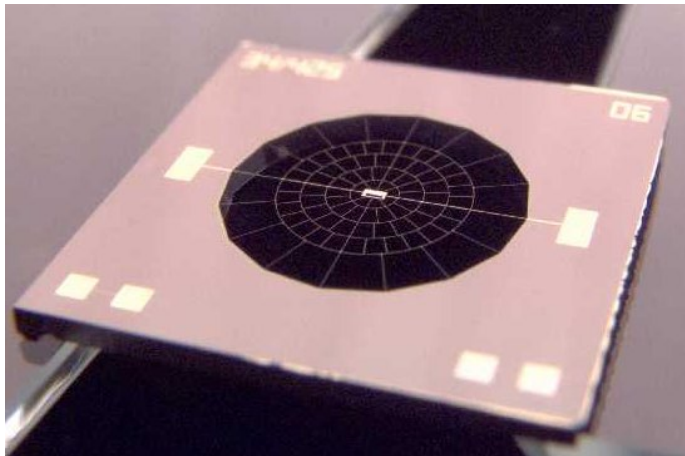
PLANCK Focal Plane



Polarization Sensitive Bolometers



Spiderweb Bolometer

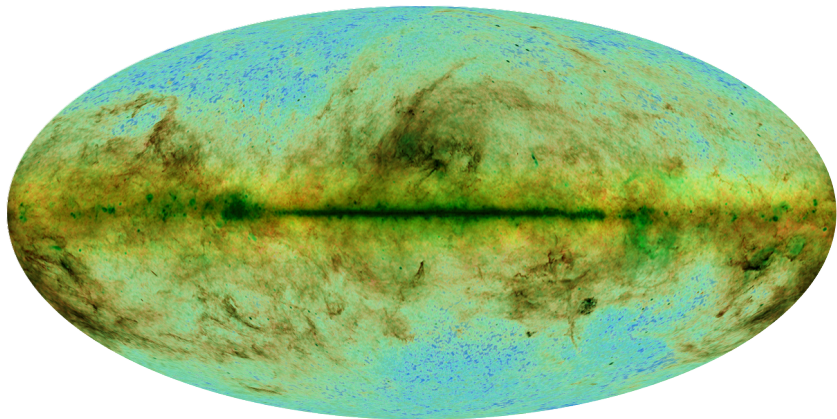


Planck Capabilities

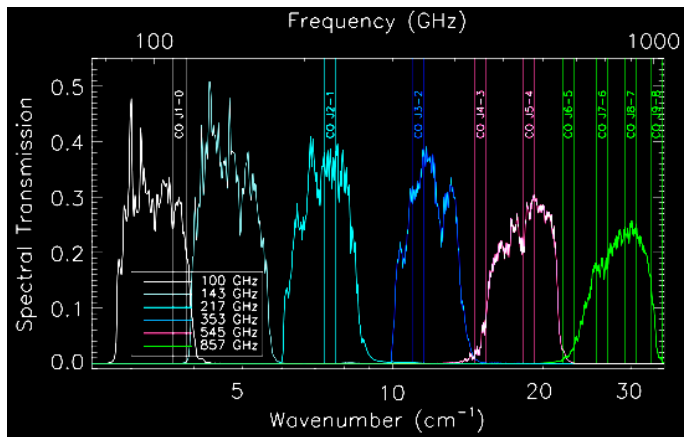
ν GHz	n_{unpol}	n_{pol}	θ_{fwhm} arcmin	Temp (I) $\mu K \cdot \text{arcmin}$		Pol (Q,U) $\mu K \cdot \text{arcmin}$	
				RJ	CMB	RJ	CMB
30	4	4	32.7	198.5	203.2	280.7	287.4
44	6	6	27.9	228.0	239.6	322.4	338.9
70	12	12	13.0	186.5	211.2	263.7	298.7
100	8	8	9.9	23.9	31.3	33.9	44.2
143	11	8	7.2	11.9	20.1	19.7	33.3
217	12	8	4.9	9.4	28.5	16.3	49.4
353	12	8	4.7	7.6	107.0	13.2	185.3
545	3	0	4.7	6.8	1.1×10^3	—	—
857	3	0	4.4	2.9	8.3×10^4	—	—

PLANCK (30 month mission)

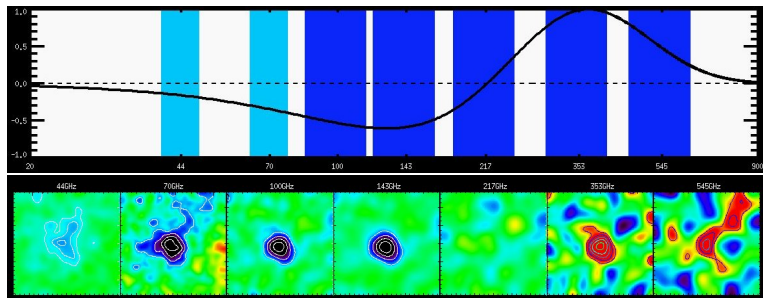
Planck Sky



Planck Frequency Bands



Sunyaev-Zeldovich Effect (Clusters of Galaxies)



New effects take over at large ℓ

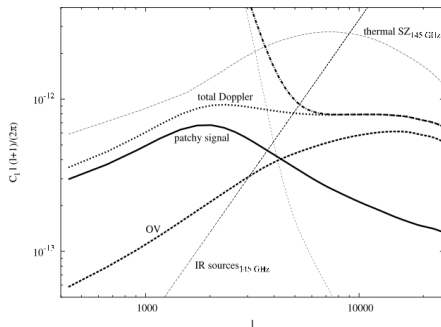
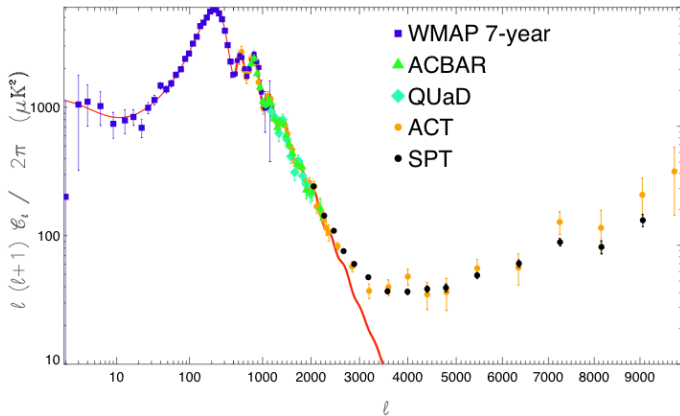
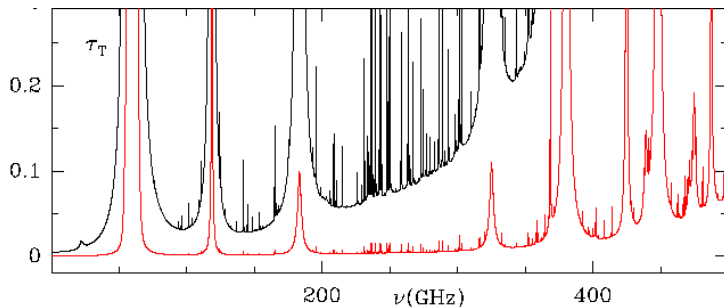


FIG. 8.— Different contributions to the total Doppler signal (kinetic SZ) in our extended patchy reionization Model C. The solid curve is the contribution to temperature anisotropies from the patchy regime alone at $z = 7 - 20$. The dashed curve gives the Doppler effect from density modulations at homogeneous ionization out to $z = 11$. The dotted curve sums up those contributions to the total Doppler signal. The total temperature fluctuations, cleaned of the thermal SZ and IR sources (shown at 145 GHz in the thin dashed lines), is given by the dot-dashed curve. These curves are smoothed versions of the power spectra generated from 50 maps.

Results at high- ℓ ACT/SPT



Observations from the Ground (I)



Atmospheric interference. Calculated optical depth through the atmosphere for a good ground-based site like the South Pole or Dome-C in Winter (black) and at balloon altitude (red). Frequency bands for sub-orbital experiments must be carefully chosen to avoid the emission by molecular lines. Moreover, emission from oxygen lines is circularly polarized and care must be taken to avoid a significant polarized signal from the tails of these lines.

Observations from the Ground (II)

Numerous CMB polarization experiments from the ground and balloons at various stages : QUaD, BICEP; BRAIN, CLOVER, EBEx, PAPPa, PolarBear, QUIET and Spider

- ▶ Far side lobes
- ▶ Scanning pattern (must scan at constant zenith angle)
- ▶ Polarization from interaction of Zeeman splitting by earth's magnetic field of oxygen lines. Atmospheric backscattering (very polarized) could be a serious problem. [See L. Pietranera et al., "Observing the CMB polarization through ice," MNRAS 346, 645 (2007)].
- ▶ Lack of stability and partial sky coverage

Photon shot noise

For a single mode :

$$\langle N \rangle = \left(\exp(x) - 1 \right)^{-1}, \quad x = \left(\frac{h\nu}{k_B T_{CMB}} \right) = \left(\frac{\nu}{57 \text{ GHz}} \right)$$

$$\langle N^2 \rangle = 2\langle N \rangle^2 + \langle N \rangle, \quad \langle (\delta N)^2 \rangle = \langle N \rangle^2 + \langle N \rangle = N^2 + N$$

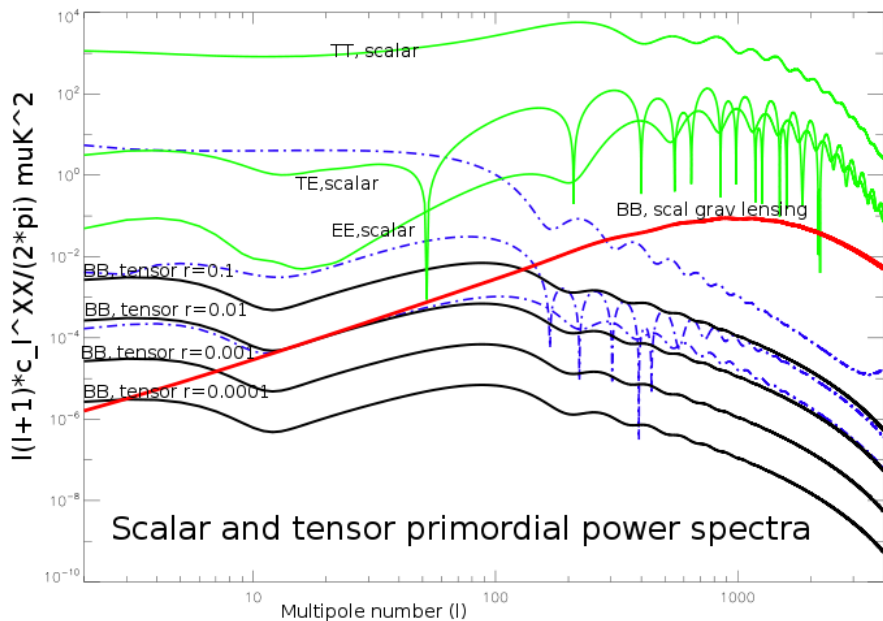
$$\left(\frac{\delta N}{N} \right) = \sqrt{1 + N^{-1}}$$

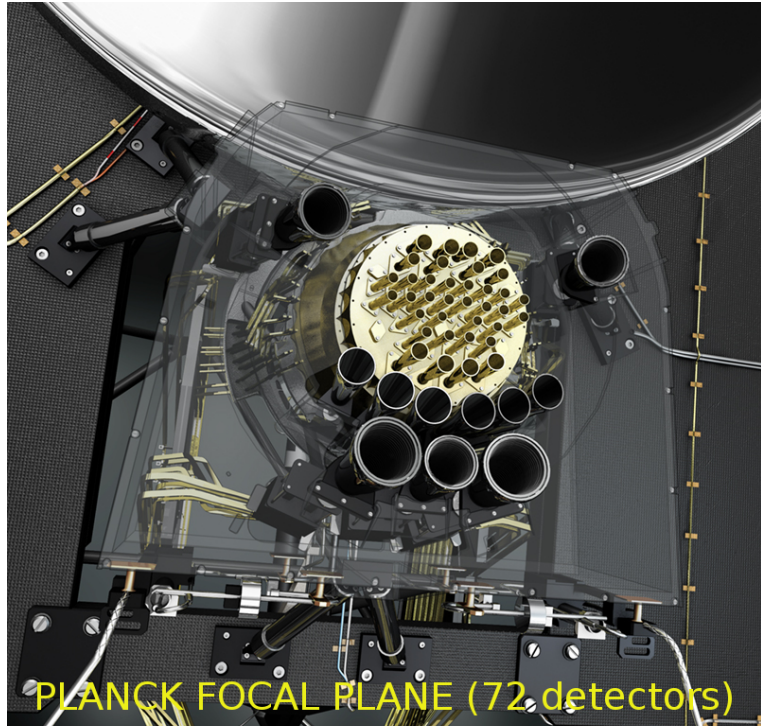
For $x \gg 1$, pure Poissonian noise, almost. For $x \ll 1$, photon bunching (Hanbury Brown and Twiss) photons arrive roughly in bunches of N , these correlations augment noise relative to Poisson distribution.

Radio astronomers' formula (quantum corrected)

$$\left(\frac{\delta I}{I} \right) = \frac{1}{\sqrt{N_{det}}} \left(\frac{T_{sky} + \epsilon_{tel} T_{tel}}{T_{sky}} \right) \frac{1}{\sqrt{(\Delta\nu)t_{obs}}} \sqrt{e^{-1} + n_{occ}^{-1}}$$

e = (quantum efficiency) = (prob. γ is absorbed), $T_{sky} \approx T_{CMB}$
 ϵ_{tel} = (telescope emissivity)



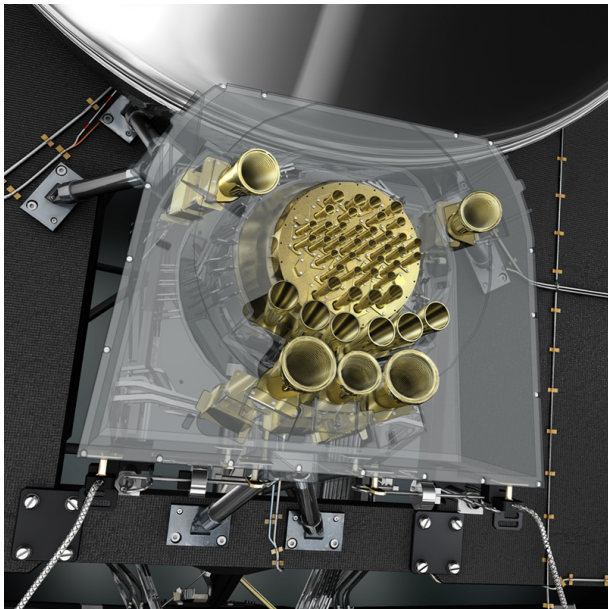


PLANCK FOCAL PLANE (72 detectors)

The *Planck* mission



PLANCK Focal Plane



A Joint Analysis of BICEP2/Keck Array and Planck Data BICEP2/Keck and Planck Collaborations 2015 Submitted

Planck intermediate results. XXX. The angular power spectrum of polarized dust emission at intermediate angular scales

Planck 2015 results. I. Overview of products and results

Planck 2015 results. II. Low Frequency Instrument data processing

Planck 2015 results. III. LFI systematic uncertainties

Planck 2015 results. IV. LFI beams and window functions

Planck 2015 results. V. LFI calibration

Planck 2015 results. VI. LFI maps

Planck 2015 results. VII. High Frequency Instrument data processing: Time-ordered information and beam parameters

Planck 2015 results. VIII. High Frequency Instrument data processing: Calibration and maps

Planck 2015 results. IX. Diffuse component separation: CMB maps

Planck 2015 results. X. Diffuse component separation: Foreground maps

Planck 2015 results. XI. CMB power spectra, likelihood, and consistency of cosmological parameters

Planck 2015 results. XII. Simulations Planck Collaboration

Planck 2015 results. XIII. Cosmological parameters

Planck 2015 results. XIV. Dark energy and modified gravity

Planck 2015 results. XV. Gravitational lensing

Planck 2015 results. XVI. Isotropy and statistics of the CMB

Planck 2015 results. XVII. Primordial non-Gaussianity

Planck 2015 results. XVIII. Background geometry and topology of the Universe

Planck 2015 results. XIX. Constraints on primordial magnetic fields

Planck 2015 results. XX. Constraints on inflation

Planck 2015 results. XXI. The integrated Sachs-Wolfe effect

Planck 2015 results. XXII. A map of the thermal Sunyaev-Zeldovich effect

Planck 2015 results. XXIII. Thermal Sunyaev-Zeldovich effect-cosmic infrared background correlation

Planck 2015 results. XXIV. Cosmology from Sunyaev-Zeldovich cluster counts

Planck 2015 results. XXV. Diffuse, low-frequency Galactic foregrounds

Planck 2015 results. XXVI. The Second Planck Catalogue of Compact Sources

Planck 2015 results. XXVII. The Second Planck Catalogue of Sunyaev-Zeldovich Sources

Planck 2015 results. XXVIII. The Planck Catalogue of Galactic Cold Clumps

<http://www.cosmos.esa.int/web/planck/publications>

Temperature (TT) power spectrum with residuals

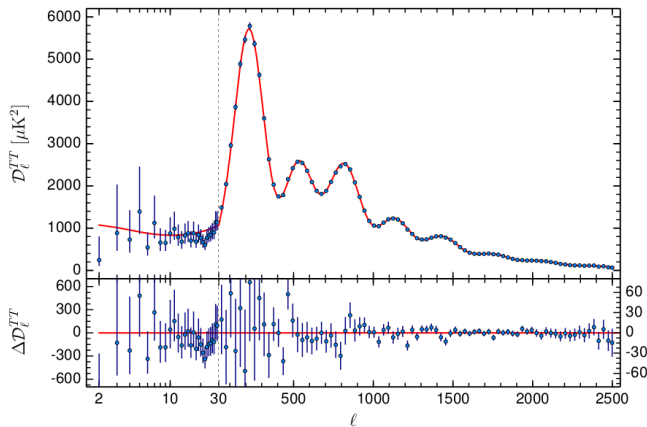
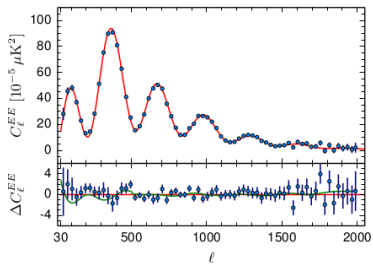
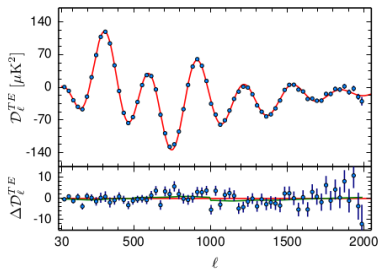


Fig. 1. The *Planck* 2015 temperature power spectrum. At multipoles $\ell \geq 30$ we show the maximum likelihood frequency averaged temperature spectrum computed from the Plik cross-half-mission likelihood with foreground and other nuisance parameters determined from the MCMC analysis of the base Λ CDM cosmology. In the multipole range $2 \leq \ell \leq 29$, we plot the power spectrum estimates from the Commander component-separation algorithm computed over 94% of the sky. The best-fit base Λ CDM theoretical spectrum fitted to the *Planck* TT+lowP likelihood is plotted in the upper panel. Residuals with respect to this model are shown in the lower panel. The error bars show $\pm 1\sigma$ uncertainties.

Polarization TE and EE spectra with residuals



The polarization PS reinforces the six-parameter orthodoxy

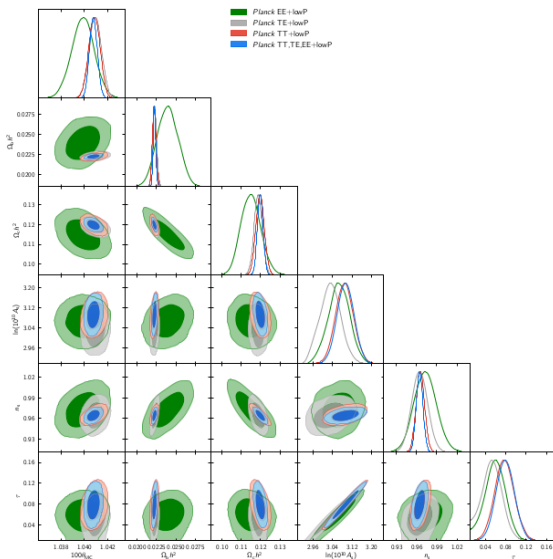


Fig. 6. Comparison of the base Λ CDM model parameter constraints from *Planck* temperature and polarization data.

Perturbations generated during inflation

$$\boxed{\hbar = c = 1, M_{pl}^{-2}} \quad \delta\phi \approx H \quad \frac{\delta\rho}{\bar{\rho}} \approx H \cdot \delta t, \quad \delta t \approx \frac{\delta\phi}{\dot{\phi}}$$

$$H\dot{\phi} \approx V_{,\phi}, \quad \dot{\phi} \approx V_{,\phi}/H, \quad H^2 \approx \frac{1}{M_{pl}^2} V, \quad \frac{\delta\rho}{\bar{\rho}} \approx \frac{V^{3/2}[\phi(k)]}{M_{pl}^3 V_{,\phi}}$$

Scalar perturbations :

$$\mathcal{P}_S^{1/2}(k) \approx O(1) \cdot \frac{V^{3/2}[\phi(k)]}{M_{pl}^3 V_{,\phi}[\phi(k)]}.$$

Tensor perturbations :

$$\mathcal{P}_T^{1/2}(k) \approx O(1) \cdot \frac{H}{M_{pl}} \approx O(1) \cdot \frac{V^{1/2}}{M_{pl}^2}$$

$\phi(k) \equiv$ value of ϕ at horizon crossing of the mode k

Reconstruction of the inflationary potential : the tensors measure the height of the potential, the scalars the slope.

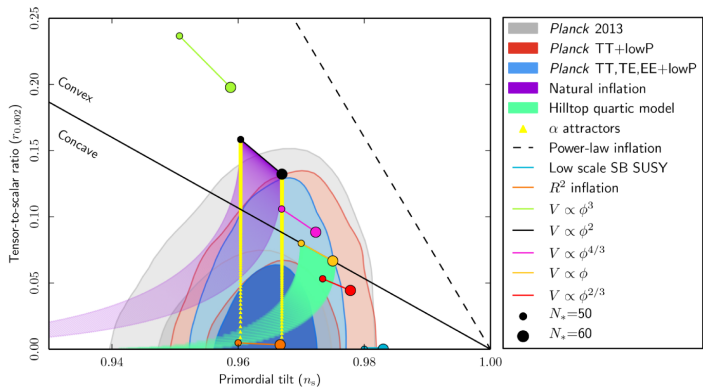


Fig. 12. Marginalized joint 68 % and 95 % CL regions for n_s and $r_{0.002}$ from *Planck* in combination with other data sets, compared to the theoretical predictions of selected inflationary models.

Underlying question : conventional parameterization

What is the primordial power spectrum ?

- For lack of a fundamental theory, expand in powers of $\ln(k)$

$$\begin{aligned}\ln(\mathcal{P}(\ln k)) &= \mathcal{P}_0 \left(\ln(k/k_{piv}) \right)^0 + \mathcal{P}_1 \left(\ln(k/k_{piv}) \right)^1 + \mathcal{P}_2 \left(\ln(k/k_{piv}) \right)^2 + \dots \\ \mathcal{P}(k) &= A(k/k_{piv})^{(n_s-1)} \\ \text{or} \\ \mathcal{P}(k) &= A(k/k_{piv})^{(n_s-1)+\alpha \ln(k/k_{piv})+\dots}\end{aligned}$$

- *Planck* seems to be telling us that the first two terms suffice, and using just the first term can be ruled out at a respectable statistical significance. $n_s \neq 1$ implies exact scale invariance needs to be downgraded to an approximate symmetry. No statistically significant evidence for running of the spectral index.

Penalized likelihood

$$\mathbf{f}^T \mathbf{R}(\lambda, \alpha) \mathbf{f} \equiv \lambda \int \mathrm{d}\kappa \left(\frac{\partial^2 f(\kappa)}{\partial \kappa^2} \right)^2 \\ + \alpha \int_{-\infty}^{\kappa_{\min}} \mathrm{d}\kappa f^2(\kappa) + \alpha \int_{\kappa_{\max}}^{+\infty} \mathrm{d}\kappa f^2(\kappa).$$

$$\kappa = \ln(k), \quad f(\kappa) = A_S k^{n_S} [1 + f(k)]$$

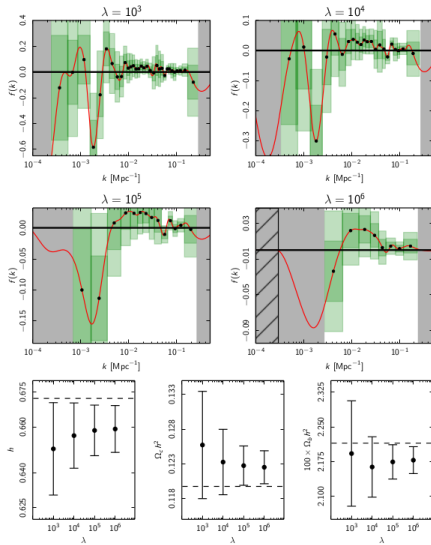


Fig. 21. *Planck* TT likelihood primordial power spectrum (PPS)

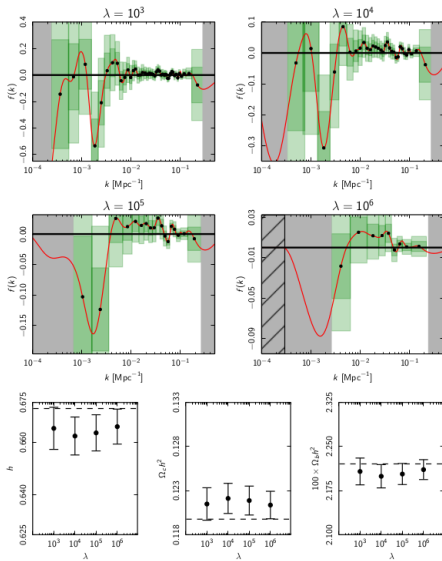
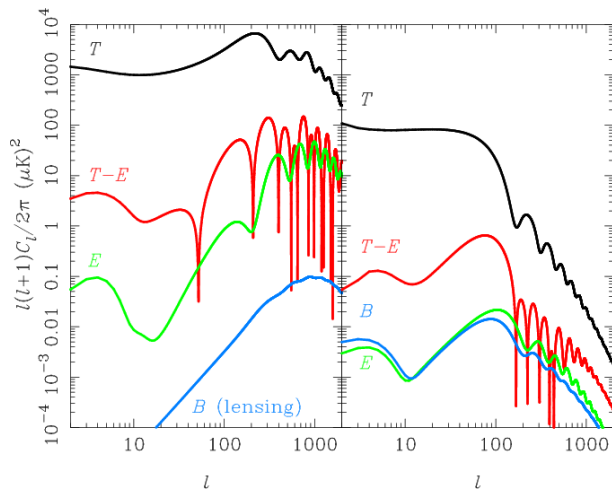


Fig. 22. *Planck* TT,TE,EE+lowTEB likelihood primordial power spectrum reconstruction results. *Top four panels:*

Constraining tensor modes

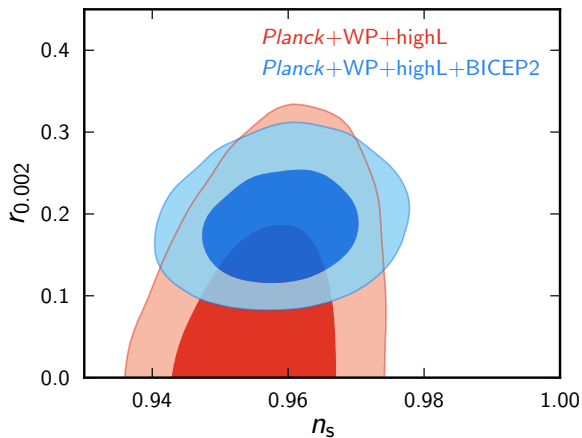
Detecting tensor modes with the CMB TT power spectrum



$r=0.24$

Taken from : Challinor, astro-ph/1210.6008

BICEP2 claim on Planck-like plot



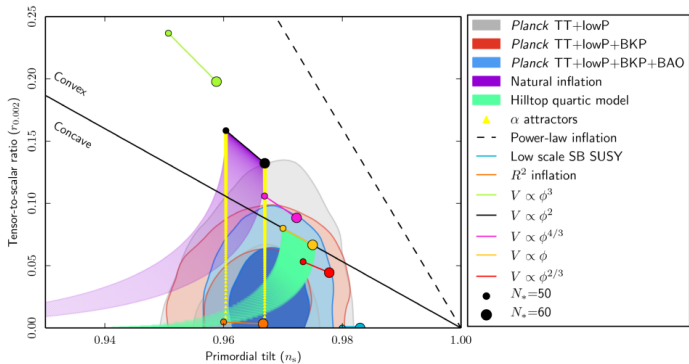


Fig. 54. Marginalized joint 68 % and 95 % CL regions for n_s and $r_{0.002}$ from *Planck* alone and in combination with its cross-correlation with BICEP2/Keck Array and/or BAO data compared with the theoretical predictions of selected inflationary models.

Constraining tensors with B modes :
A clean probe

E and B Mode Polarization



E mode

B mode

$$\mathbf{Y}_{\ell m, ab}^{(E)} = \sqrt{\frac{2}{(\ell-1)\ell(\ell+1)(\ell+2)}} \left[\nabla_a \nabla_b - \frac{1}{2} \delta_{ab} \nabla^2 \right] Y_{\ell m}(\hat{\Omega})$$

$$\mathbf{Y}_{\ell m, ab}^{(B)} = \sqrt{\frac{2}{(\ell-1)\ell(\ell+1)(\ell+2)}} \frac{1}{2} \left[\epsilon_{ac} \nabla_c \nabla_b + \nabla_a \epsilon_{bc} \nabla_c \right] Y_{\ell m}(\hat{\Omega})$$

Projection of « scalars, » « vectors » and « tensors » onto the celestial sphere

Under projection onto the celestial sphere :

$$(scalar)_3 \rightarrow (scalar)_2,$$

$$(vector)_3 \rightarrow (scalar)_2 + (vector)_2,$$

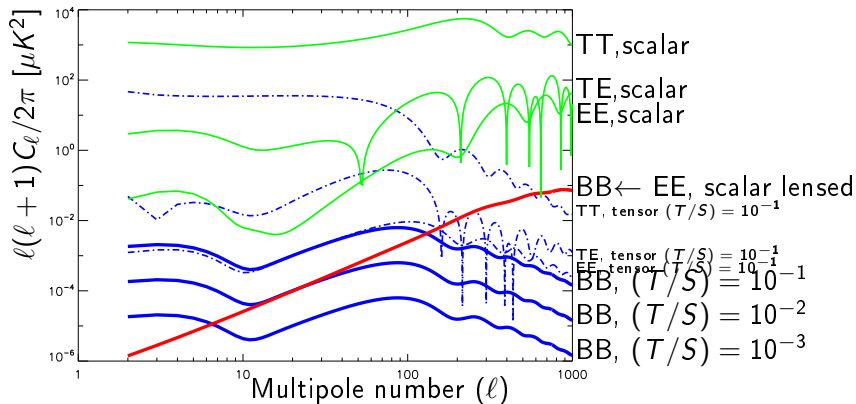
$$(tensor)_3 \rightarrow (scalar)_2 + (vector)_2.$$

There is no $(tensor)_2$ component. The E mode polarization is scalar; the B mode is vector.

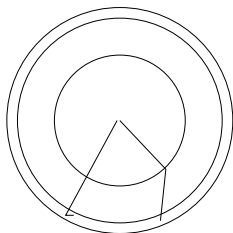
It follows that at linear order the scalar modes cannot generate any B mode polarization.

Note crucial role of linearity assumption.

Inflationary Prediction for Scalar & Tensor Anisotropies



The Reionization Bump



It turns out that

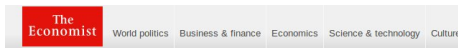
$$P \propto (1 - \tau) d_{\text{lastscatter}}^2 \frac{\partial^2 T}{\partial x^2}$$

is small compared to

$$P \propto \tau d_{\text{reion}}^2 \frac{\partial^2 T}{\partial x^2}$$

even when τ is small.

Breaking news 22 March 2014



Astrophysics

BICEP flexes its muscles

A telescope at the South Pole has made the biggest cosmological discovery so far this century

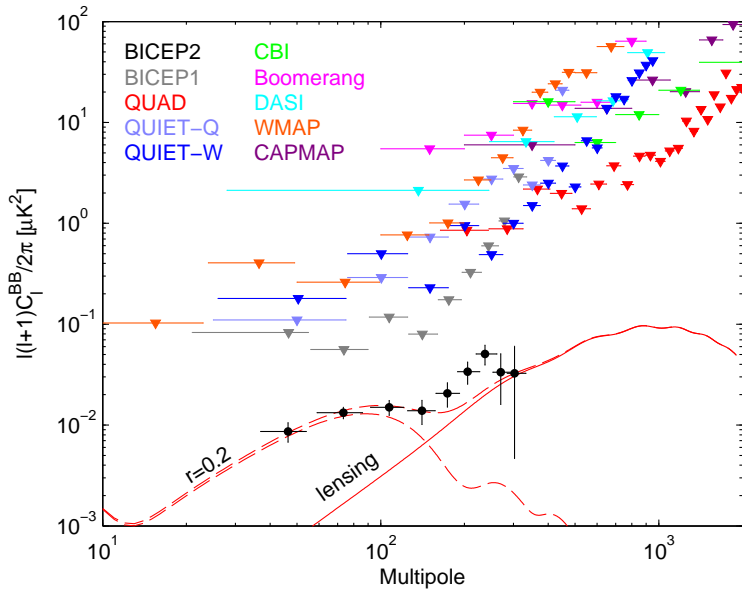
Mar 22nd 2014 | From the print edition

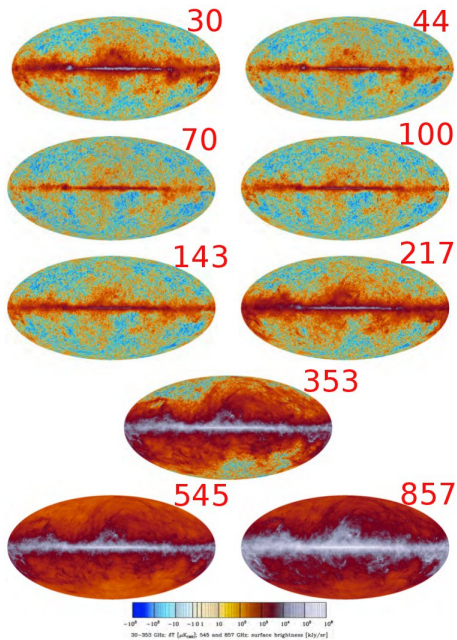


ONE useful feature of a scientific theory is that it makes testable predictions. Such predictions, though, do not have to be testable straight away. Physics is replete with prophecies that could be confirmed or denied only decades later, once the technology to examine them had caught up. The Higgs boson, for example, was 50 years in the confirming.

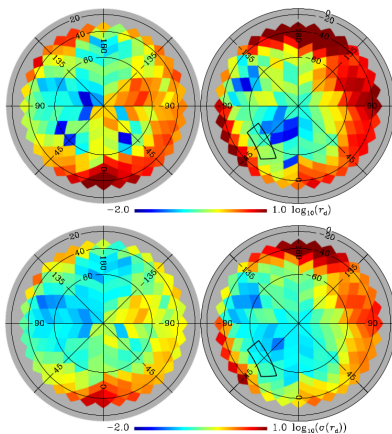
BICEP2 summary plot :

"Smoking gun" of gravitational waves from inflation?

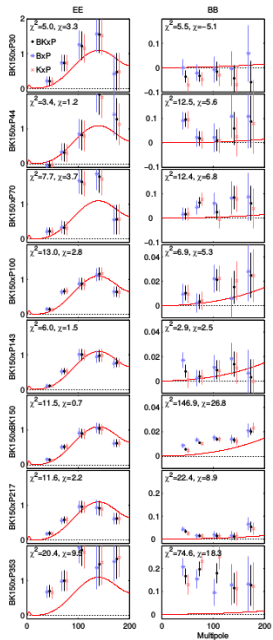




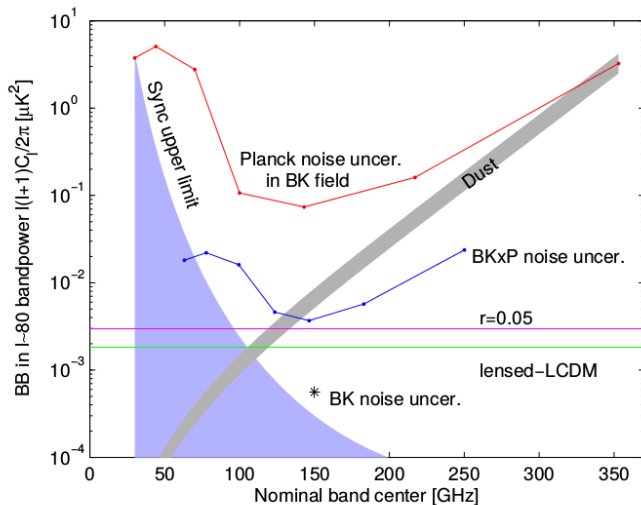
Planck Collaboration: Dust polarization at high latitudes



From Planck Collaboration : Dust polarization at high latitudes
(astro-ph/1409.3738)



$r < 0.12$ at 95 % now from B modes



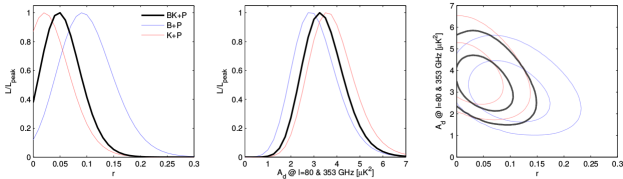


FIG. 6. Likelihood results from a basic lensed- Λ CDM+ r +dust model, fitting BB auto- and cross-spectra taken between maps at 150 GHz, 217, and 353 GHz. The 217 and 353 GHz maps come from *Planck*. The primary results (heavy black) use the 150 GHz combined maps from BICEP2/*Keck*. Alternate curves (light blue and red) show how the results vary when the BICEP2 and *Keck Array* only maps are used. In all cases a Gaussian prior is placed on the dust frequency spectrum parameter $\beta_d = 1.59 \pm 0.11$. In the right panel the two dimensional contours enclose 68% and 95% of the total likelihood.

LiteBIRD

A focused mission for discovering B modes from inflation



LiteBIRD

Lite (Light) Satellite for the studies of **B**-mode polarization and **I**nflation from cosmic background **R**adiation **D**etection (<http://litebird.jp/>)

LiteBIRD is a next generation scientific satellite aiming to measure polarization of Cosmic Microwave Background (CMB) at unprecedented sensitivity.

Mission Requirements:

- Measurement of B-mode polarization spectrum of large angular scale (by three-year observation of all sky).
- Measurement of the tensor-to-scalar ratio r , that represents primordial gravitational waves, at precision $\sigma_r < 0.001$ (w/o subtracting the gravitational lensing effect.)

JAXA

T. Dotani
H. Fuke
H. Imada
I. Kawano
H. Matsuhara → IPMU
T. Matsumura
K. Mitsuda
T. Nishibori
K. Nishijo
A. Noda
A. Okamoto
S. Sakai
Y. Sato
K. Shinozaki
H. Sugita
Y. Takei
S. Utsunomiya
T. Wada
R. Yamamoto
N. Yamasaki
T. Yoshida
K. Yotsumoto

Osaka U.

S. Kuromiya
M. Nakajima
S. Takakura
K. Takano

Osaka Pref. U.

M. Inoue
K. Kimura
H. Ogawa
N. Okada

Okayama U.

T. Funaki
N. Hidehira
H. Ishino
A. Kibayashi
Y. Kida
K. Komatsu
S. Uozumi
Y. Yamada

NIFS

S. Takada

Kavli IPMU

K. Hattori
N. Katayama
Y. Sakurai
H. Sugai

KEK

M. Hazumi (PI)
M. Hasegawa
N. Kimura
K. Kohri
M. Maki
Y. Minami
T. Nagasaki
R. Nagata
H. Nishino
S. Oguri
T. Okamura
N. Sato
J. Suzuki
T. Suzuki
O. Tajima
T. Tomaru
M. Yoshida

Kansei

Gakuin U.
S. Matsuura

Kitazato U.

T. Kawasaki

Konan U.

I. Ohta

NAOJ

A. Dominjon
T. Hasebe
J. Inatani
K. Karatsu
S. Kashima
T. Noguchi
Y. Sekimoto
M. Sekine

Saitama U.

M. Naruse

NICT

Y. Uzawa

SOKENDAI

Y. Akiba
Y. Inoue
H. Ishitsuka
Y. Segawa
S. Takatori
D. Tanabe
H. Watanabe

U. Tsukuba

M. Nagai

TIT

S. Matsuoka
R. Chendra

U. Tokyo

S. Sekiguchi
T. Shimizu
S. Shu
N. Tomita

Tohoku U.

M. Hattori

Nagoya U.

K. Ichiki

Yokohama

Natl. U.

T. Fujino
F. Irie
H. Kanai
S. Nakamura
T. Yamashita

RIKEN

S. Mima
C. Otani

APC Paris

J. Errard
R. Stompore

Cardiff U.

G. Pisano

CEA

L. Duband
J.M. Duval

CU Boulder

N. Halverson

McGill U.

M. Dobbs

MPA

E. Komatsu

NIST

G. Hilton
J. Hubmayr

Stanford U.

S. Cho
K. Irwin
S. Kerasovskiy
C.-L. Kuo
D. Li
T. Namikawa
K. L. Thompson

UC Berkeley /

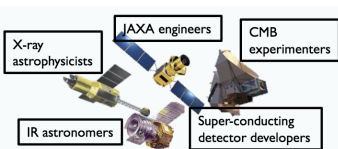
LBNL

D. Barron
J. Borrill
Y. Chinone
A. Cukierman
D. Curtis
T. de Haan
L. Hayes
J. Fisher
N. Goeckner-wald
C. Hill
O. Jeong
R. Keskitalo
T. Kisner
A. Kusaka
A. Lee (US PI)
E. Linder
D. Meilhan
P. Richards
E. Taylor
U. Seljak
B. Sherwin
A. Suzuki
P. Turin
B. Westbrook
M. Willer
N. Whitehorn

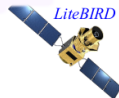
UC San Diego

K. Arnold
T. Elleot
B. Keating
G. Rebeiz

LiteBIRD working group



139 members, international and interdisciplinary (as of May 1, 2016) 5

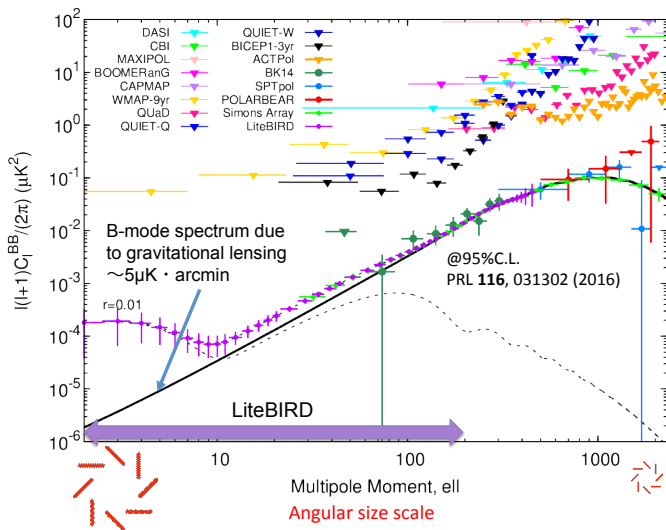


Global schedule

Development model with
Demonstration Model (DM),
Engineering Model (EM) and
Flight Model (FM).

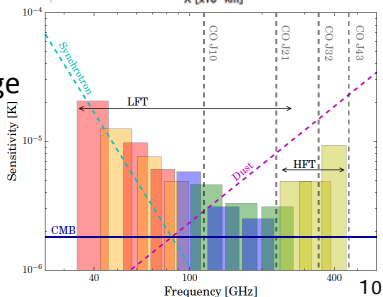
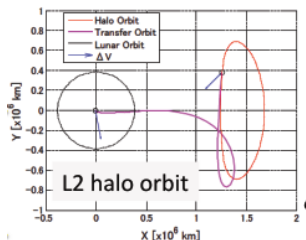
Phase A1 end	2018 Sep.
SRR	2018 end
final selection	2019
Phase A2/B (DM)	2019-2020
Phase C (EM)	2021-2022
Phase C (FM)	2023-2025
Launch	2026

LiteBIRD Measurement Precision (at $r=0.01$)

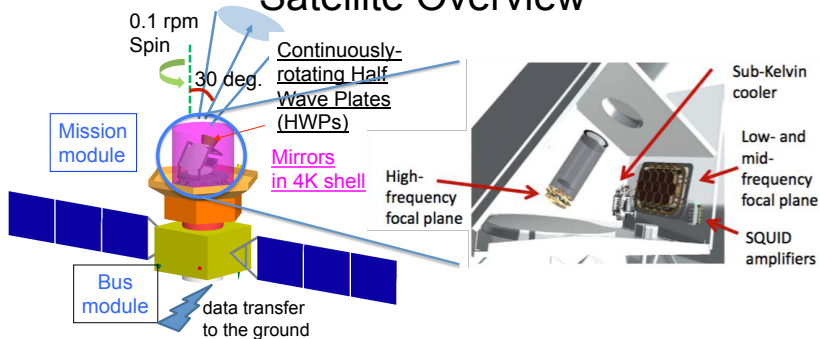


Mission specification

- Operation at Lagrange-point 2
- Full-sky scan
- Optimized for large-angle polarization structure from primordial B-mode signal
- High detector sensitivity:
3 $\mu\text{K arcmin}$ with margin
- Wide frequency band coverage (40-400 GHz, 15 bands)
- Launch around 2025-2027
- 3 years operation

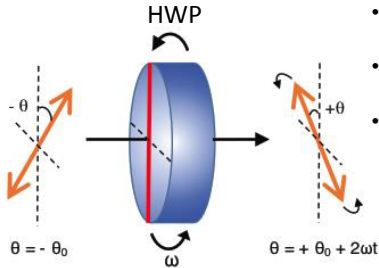


Satellite Overview



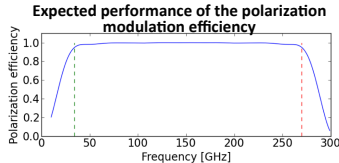
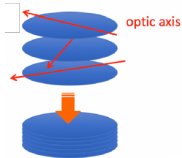
- Satellite consists of two modules : low-temp. mission part and normal-temp bus part.
- Rotating HWP modulates incoming signal.
- Two complementary optics : LFT and HFT to cover wide freq. bands.
- Optics are kept under 4K by JT/ST and ADR cryogenics.
- Superconducting detectors (TES) are arranged on focal planes.

Rotating Half Wave Plate

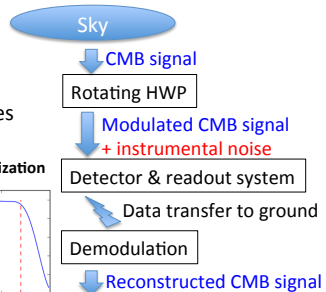


JPS_Sep2016_23aSR-9, Sakurai et al.

- Stacking several layers of rotating HWP makes freq. bandwidth wider.



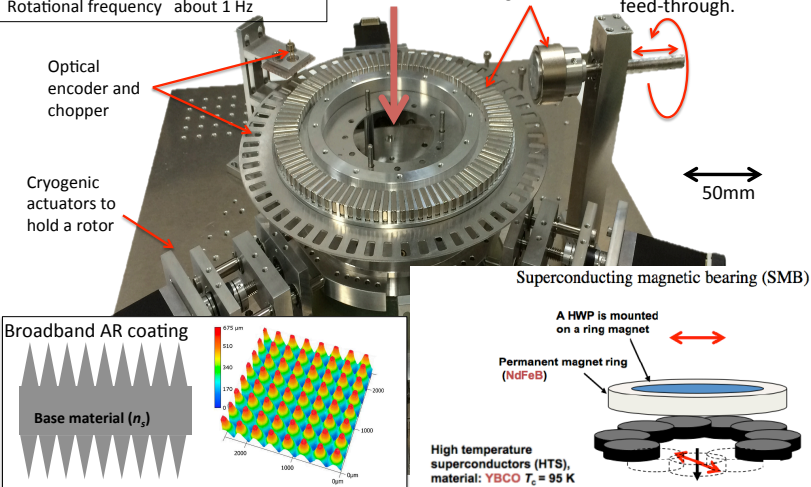
- HWP changes direction of polarization with respect to a fixed axis.
- Modulation of CMB signal by rotating HWP reduces $1/f$ noise.
- Other instrumental systematics can be greatly reduced by rotating HWP.



HWP Small diameter prototype rotational mechanism

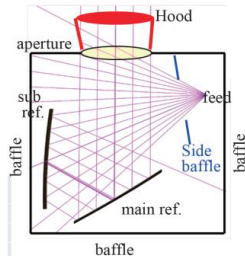
Aperture (a half-wave plate diameter)
 $\Phi 50\text{mm}$
Operation temperature $<10\text{ K}$
Rotational frequency about 1 Hz

The shaft is coupled to a motor mounted outside of the cryostat via linear/rotational feed-through.

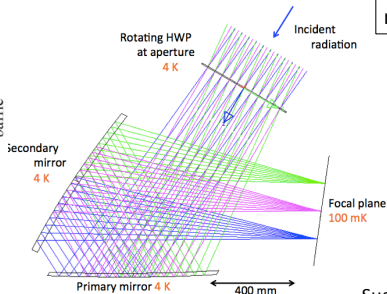


Optical System

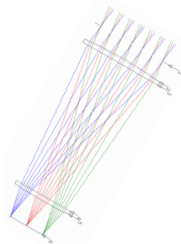
- Beam size : < 1 deg. at all the observing band
- FOV: 10 x 20 degs.
- Aperture Size: 40cm
- Covered by 4K shell
- Cold Baffle and Mirrors



Low-Frequency Telescope (LFT)
Crossed-dragon compact structure



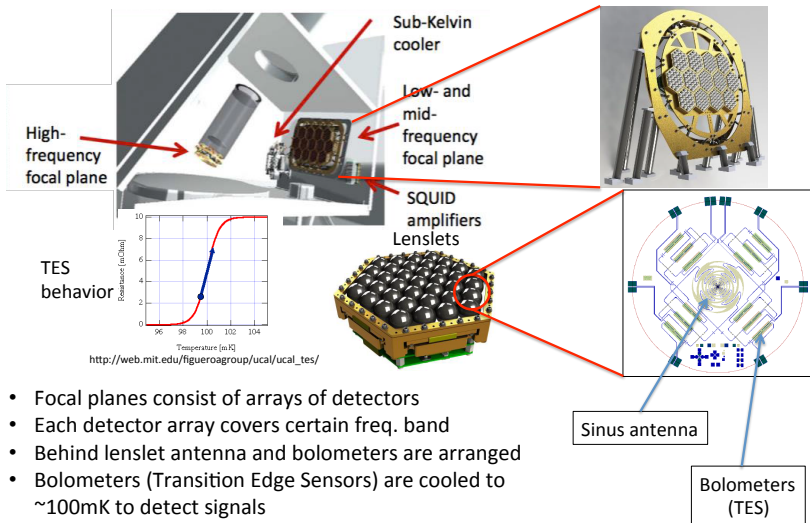
High-Frequency
Telescope (HFT)
refractive telescope



Sugai et al. (2016)

14

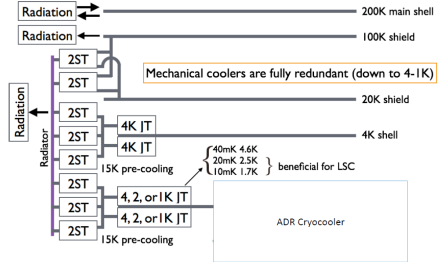
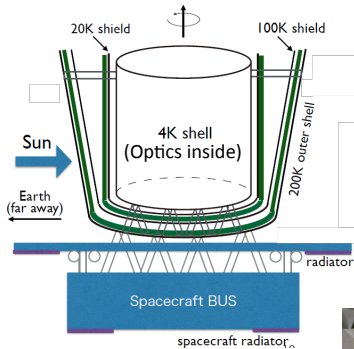
Focal Plane Detectors



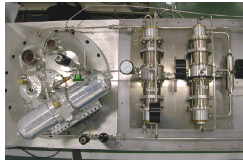
- Focal planes consist of arrays of detectors
- Each detector array covers certain freq. band
- Behind lenslet antenna and bolometers are arranged
- Bolometers (Transition Edge Sensors) are cooled to $\sim 100\text{mK}$ to detect signals
- Signal readout from Bolometer by SQUID

Cryogenic system

Cryogenic system above 2 K



- Cryogenic system consists of JT/ST and ADR coolers.
- Covering optics in 4K shell is important to reduce thermal noise.

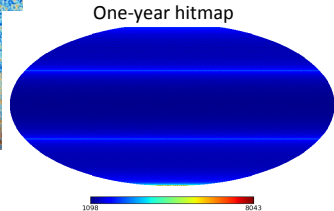
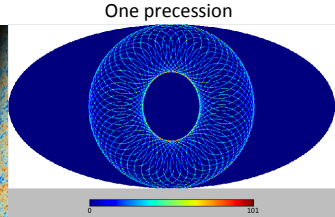
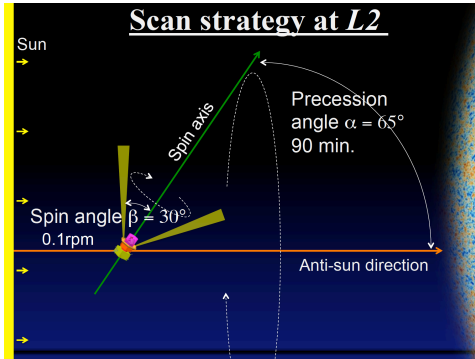


JT and ST coolers



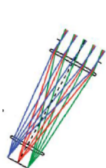
ADR cryocooler

All Sky Scan Strategy

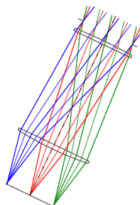


- Precession + spin angle < 95 deg. for full anti-sun direction scan
- Satellite scans all sky at L2 combining “precession” and “spin” motion

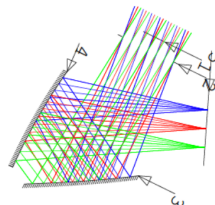
HFT design examples



Original design



Large refractive design
(LO-HFT300)



Reflective design
(CD-HFT300)

Optics design by Shingo Kashima

Model	Aperture Diameter [mm]	$F/\#$	Field of view [deg ²]	Focal plane area [mm ²]
Original design	200	2.2	ϕ 13	ϕ 102
Large refractive design	300	2.2	ϕ 24	ϕ 280
Reflective design	300	3.5	20×10	370×184

